Journal of Computational and Theoretical Nanoscience Vol.5, 2008 (*in press*)

Targeting Transport Properties in Nanofluidics: Hydrodynamic Interaction Among Slip Surface Nanoparticles in Solution

Kengo Ichiki,[1,2] Alexander E. Kobryn,[2] and Andriy Kovalenko[2,1,*]

[1]*Department of Mechanical Engineering, University of Alberta, Edmonton, AB, T6G 2G8, Canada*
[2]*National Institute for Nanotechnology, National Research Council of Canada, 11421 Saskatchewan Drive, Edmonton, AB, T6G 2M9, Canada*

(Dated: July 29, 2008)

Hydrodynamic interaction among rigid nanoparticles in laminar flow with Navier's slip boundary condition on the nanoparticles' surfaces is formulated. The single-particle problem under the general linear flow is solved in terms of the Lamb general solution, and the velocity field exerted by the slip particle is expressed in terms of the multipole expansion in the force moments. Thereby, the mobility matrix for a many-body system is constructed with Faxén's laws for the force, torque and the stresslet, and is extended to periodic systems by the Ewald summation technique. Using this formulation, the Stokesian dynamics method is generalized to slip particles with arbitrary slip length. The method is applied to a system in an unbounded fluid and to a system with periodic boundary conditions. The mobility problem with constant force for the former and sedimentation velocity (drag coefficient) and spin and shear viscosities for the latter are solved. A comparison is made with the existing results for no-slip particles. According to the surface slip, the reductions of friction (drag force), spin and shear viscosities are observed for the problems with the applied force, torque, and shear, respectively. In particular, we show that just changing the slip properties of the nanoparticle surface, one can control the drag force within an order of magnitude. The slip-length dependences of the drag coefficient and other rheological properties are useful for rational design of nanofluidic devices, including controllable manipulation and separation of large biomolecules in nanofluidic channels.

Keywords: Nanofluidics, Slip Boundary Condition, Hydrodynamic Interaction, Stokes Flow.

I. INTRODUCTION

Microfluidics and nanofluidics enable analytical methods and devices for controlling and manipulating fluid flows at small length scales.[1–4] For nanoparticles, it is typically less than a micrometer. This subject has recently received an enormously large attention by growing interests to the nanotechnology and its application in biophysics, biochemistry and medicine. In nanofluidic devices, the hydrodynamic interaction of the target object to the system boundary through the fluid dominates the intermolecular interactions. Because changing the shape and/or the material of the instrumentality is feasible and that changing intrinsic intermolecular forces is not, nanofluidic devices turned to be much more flexible to control the system function than conventional experimental setups where the bulk character of the fluid dominates. Illustrative examples where it can be used are given by experiments on separation[5–7] and single molecule detection[8–10] of biomolecules. One of the important mechanisms in these processes is the hydrodynamic interaction.

At present, study in the field is driven largely by experimental works, and there is a general lack of theoretical research. For further progress and breakthrough, it is inevitable to understand physics of processes in fluids in nanometer scale by theoretical framework based on solid foundation capable of explaining the existing results and of predicting new phenomena that might happen in such devices. A possible theoretical account combines hydrodynamic and statistical mechanical theories. The focus of this article is the former, which describes the fluid flows by the Stokes equation and uses a single parameter called the "slip length" characterizing the boundary condition in the nano scale. At this point, it is worth to note that, at least for straight channel flows, molecular dynamics simulations confirmed that the hydrodynamic theory works at the scale larger than 10 molecular diameters.[11]

Hydrodynamic interaction in Stokes flow has been actively studied in fluid mechanics[12,13] and successfully applied for colloidal suspensions and polymer solutions.[14] A typical length scale there is down to only micrometers. The interaction is obtained by solving the boundary value problem on the surface of the objects on which the conventional no-slip boundary condition is applied. Because of the long-range and many-body nature of the interaction, computational methods are not just a numerical tool but an important theoretical component for understanding the physics. There exist a variety of numerical formulations: Among them, boundary element method is widely used for deformable objects,[15] and Stokesian dynamics method is for solid particles.[16–19] Usually, calculations of full hydrodynamic interaction is computationally heavy, although several improvements have been proposed to ease the heavy load.[20–22] Because of the computational cost, in several practical occasions, hydrodynamic interaction is often ignored or replaced by a simpler form (like the point force approximation) or empirical mesoscopic models such as dissipative particle dynamics.[23] However, for the present purpose of establishing the theoretical framework for nanofluidics, where the hydrodynamics has an important role, we should not compromise on it.

One of the problems of the application of the hydrodynamic theory in Stokes flows for nanofluidics is on the no-

*Electronic address: andriy.kovalenko@nrc-cnrc.gc.ca

slip boundary condition. Recently, by the ability to probe small length scales and to fabricate surfaces with various properties, apparent violations of the no-slip boundary condition at the liquid-solid interface in nano scale have been reported even for simple liquids.[24–27] The slip boundary condition was first proposed by Navier[28] in 19th century, the early age of fluid mechanics, when the proper boundary conditions (mainly between no-slip and partial-slip) were discussed in the first place.[25] For gas flows, Maxwell had shown that the surface slip is related to the non-continuous nature of gas and the slip length is proportional to the mean-free path.[29] For liquids, on the other hand, from experiments at that age the no-slip boundary condition was accepted by the 1900s, and since then had been treated as a fundamental law. By recent extensive studies on the surface slip in micro and nano scales, the physics of the liquid-solid slip is realized to be much more complicated than that for gases. There are many factors which would affect the surface slip including individual molecular interaction, surface roughness, surface charge, and wetting condition, and at this stage it is too early to make any conclusive consensus about the physics of the liquid-solid slip.[24,30]

In this article, we focus on the formulation of the hydrodynamic interaction among rigid spherical particles with arbitrary slip length, and therefore, this formulation is applicable to nanofluidic situations. We also extend the Stokesian dynamics method for slip particles in terms of the theory. The formulation in this article is limited to spherical objects. However, using spheres as building blocks to form a desired object, we are able to simulate motions of polymer chains (as well as more complex structures) in fluid flow. Moreover, systems with confined geometries such as a porous medium can be simulated by mimicking them with particles fixed in space.[31] The point of these applications is that the hydrodynamic interaction among those objects is fully taken into account, although the modeling of objects by spheres has its own limitation.

The paper is organized as follows: In Sec. II, we describe hydrodynamic interaction among spherical particles with arbitrary slip length. The results are implemented in the Stokesian dynamics method. In Sec. III, we present the numerical solutions for particles in unbounded fluid as well as particles in the cubic array configuration with the periodic boundary condition, and discuss the results. The conclusions of this article are presented in Sec. IV.

II. HYDRODYNAMICS FOR SLIP PARTICLES

In low-Reynolds number flows such as liquid flows in nanofluidic devices, the fluid motion is governed by the Stokes equation

$$-\boldsymbol{\nabla} P + \mu \nabla^2 \boldsymbol{u} = \boldsymbol{0}, \tag{1}$$

with the incompressibility condition $\boldsymbol{\nabla} \cdot \boldsymbol{u} = 0$, where P is the pressure, μ is the viscosity, and $\boldsymbol{u}$ is the velocity of the fluid. The problem of fluid mechanics is given by the boundary value problem at the boundary of the fluid. On the liquid-solid interface, there are two types of the boundary conditions, no-slip and (partial) slip. In most cases in fluid mechanics, the former is widely used, while the latter is recently getting attention especially at small scale fluid flows.[24–27]

The slip boundary condition had been proposed in such long time ago, however, the solutions are very limited, compared with those for the no-slip boundary conditions: Basset solved the flow of single particle with slip surface,[32] Felderhof solved the problems for single particle[33] and two particles,[34] Bławzdziewicz *et al.* showed the interaction between the slip particles and lubrication functions for the axisymmetric motion for the study of surfactant-covered drops,[35] and Luo and Pozrikidis studied two slip spheres under the shear flow.[36] The point force solution in semi-infinite space with a flat plane obtained by Blake[41] for no-slip condition was recently extended to the slip condition by Lauga and Squires.[30] The extension of the exact two-body solution for no-slip particles[37] to the slip particles was done by Ying and Peters[38] for the gas-solid system and by Keh and Chen[39] and one of the present author[40] for the liquid-solid system.

In this section, we briefly review the boundary conditions, and give the single-body solution of the Stokes equation under the general linear flows. For many-body problem, we construct the mobility matrix obtained by the multipole expansion of the velocity field and Faxén's laws for the force, torque, and stresslet. Finally, the formulation is extended to the periodic systems in terms of Ewald summation technique.

A. Navier's Boundary Condition

The conventional no-slip boundary condition for the velocity field $\boldsymbol{u}$ on a surface S is given by

$$\left[\boldsymbol{u} - \boldsymbol{u}^{\mathrm{S}}\right](\boldsymbol{y}) = \boldsymbol{0} \quad \text{for } \boldsymbol{y} \in S, \tag{2}$$

where $\boldsymbol{u}^{\mathrm{S}}$ is the velocity of the surface. For a rigid spherical particle with the translational velocity $\boldsymbol{U}$ and angular velocity $\boldsymbol{\Omega}$, it is given by

$$\boldsymbol{u}^{\mathrm{S}}(\boldsymbol{y}) = \boldsymbol{U} + \boldsymbol{\Omega} \times (\boldsymbol{y} - \boldsymbol{x}_0), \tag{3}$$

where $\boldsymbol{x}_0$ is the center of the particle.

Instead of the no-slip boundary condition (2), Navier's slip boundary condition[28] is given by

$$\left[\boldsymbol{u} - \boldsymbol{u}^{\mathrm{S}}\right](\boldsymbol{y}) = \frac{\gamma}{\mu} (\boldsymbol{I} - \boldsymbol{nn}) \cdot (\boldsymbol{\sigma} \cdot \boldsymbol{n}), \tag{4}$$

where γ is the slip length, $\boldsymbol{I}$ is the unit tensor, $\boldsymbol{n}$ is the unit normal vector of the surface, and $\boldsymbol{\sigma}$ is the stress tensor of the fluid defined by

$$\boldsymbol{\sigma} = -P\boldsymbol{I} + \mu \left[(\boldsymbol{\nabla u}) + (\boldsymbol{\nabla u})^{\dagger}\right]. \tag{5}$$

The symbol † denotes the transposition of the tensor. Note that $(\boldsymbol{I} - \boldsymbol{nn})$ is the projection to the tangential component. This slip boundary condition (4) exhibits kinematic boundary condition for the normal component

$$\boldsymbol{n} \cdot \left(\boldsymbol{u} - \boldsymbol{u}^{\mathrm{S}}\right) = 0, \tag{6}$$

and the slip velocity for the tangential component which is proportional to the velocity gradient as

$$\begin{aligned}&(\boldsymbol{I}-\boldsymbol{nn})\cdot\left(\boldsymbol{u}-\boldsymbol{u}^{\mathrm{S}}\right)\\ &=\ \gamma(\boldsymbol{I}-\boldsymbol{nn})\cdot\left\{\boldsymbol{n}\cdot\left[(\boldsymbol{\nabla u})+(\boldsymbol{\nabla u})^{\dagger}\right]\right\}.\end{aligned}\tag{7}$$

The proportionality factor γ has the dimension of length.

B. Single Body Problem

The fluid flow around a single spherical particle with the slip surface was first described by Basset.[32,42] Here we consider a more general case and derive the solution for a sphere moving with the translational velocity $\boldsymbol{U}$ and rotational velocity $\boldsymbol{\Omega}$ in an arbitrary linear flow

$$\boldsymbol{u}^{\infty}=\boldsymbol{U}^{\infty}+\boldsymbol{\Omega}^{\infty}\times\boldsymbol{r}+\boldsymbol{E}^{\infty}\cdot\boldsymbol{r},\tag{8}$$

where $\boldsymbol{r}$ is the relative vector from the particle center to $\boldsymbol{x}$. The disturbance field (velocity relative to the imposed flow) at a position $\boldsymbol{x}$ is expressed by Lamb's general solution[12,42] as

$$\boldsymbol{u}(\boldsymbol{x})-\boldsymbol{u}^{\infty}(\boldsymbol{x})=\sum_{n}\left[\boldsymbol{\nabla}\times\boldsymbol{r}\chi_n+\boldsymbol{\nabla}\Phi_n+C_n r^2\boldsymbol{\nabla}\frac{p_n}{\mu}+D_n\boldsymbol{r}\frac{p_n}{\mu}\right],\tag{9}$$

where χ_n, Φ_n, and p_n are harmonic functions in n-th order, and the coefficients C_n and D_n are given by

$$C_n\ =\ \frac{n+3}{2(2n+3)(n+1)},\tag{10}$$

$$D_n\ =\ -\frac{n}{(2n+3)(n+1)}.\tag{11}$$

The integer n runs from $-\infty$ to ∞ in general, but for the outer problem where the solution goes to zero at infinity, it is limited to the negative integers. The stress tensor is given by the velocity field (9) through Eq. (5). Let us expand harmonic functions by the spherical harmonics $Y_{mn}=P_n^m(\cos\theta)e^{\mathrm{i}m\phi}$ as

$$\frac{p_{-n-1}}{\mu}\ =\ \sum_{m=0}^{n}p_{mn}\frac{1}{a}\left(\frac{a}{r}\right)^{n+1}Y_{mn}(\theta,\phi),\tag{12}$$

$$\chi_{-n-1}\ =\ \sum_{m=0}^{n}q_{mn}\left(\frac{a}{r}\right)^{n+1}Y_{mn}(\theta,\phi),\tag{13}$$

$$\Phi_{-n-1}\ =\ \sum_{m=0}^{n}\nu_{mn}a\left(\frac{a}{r}\right)^{n+1}Y_{mn}(\theta,\phi),\tag{14}$$

where a is the radius of particle. The polar axis of the spherical coordinate system (r,θ,ϕ) is taken in z direction. The coefficients p_{mn}, q_{mn}, and ν_{mn} are obtained by the boundary condition (4) on the particle surface. (See Appendix A for details.)

For the translating sphere with the velocity $\boldsymbol{U}=(0,0,U)$, we have

$$p_{mn}\ =\ \frac{3}{2}U\Gamma_{2,3}\delta_{m0}\delta_{n1},\tag{15}$$

$$\nu_{mn}\ =\ \frac{1}{4}U\Gamma_{0,3}\delta_{m0}\delta_{n1},\tag{16}$$

$$q_{mn}\ =\ 0,\tag{17}$$

where factors $\Gamma_{m,n}$ represent the correction due to the surface slip and are defined as

$$\Gamma_{m,n}=\frac{1+m\widehat{\gamma}}{1+n\widehat{\gamma}}.\tag{18}$$

In definition (18), $\widehat{\gamma}$ is the scaled slip length introduced as the ratio of the slip length γ and the particle radius a:

$$\widehat{\gamma}=\frac{\gamma}{a}.\tag{19}$$

The force acting on the particle is given by the coefficients p_{mn} of Lamb's general solution as[12,37]

$$\boldsymbol{F}=4\pi\mu a\left[p_{01}\hat{\boldsymbol{z}}-p_{11}\left(\hat{\boldsymbol{x}}+\mathrm{i}\hat{\boldsymbol{y}}\right)\right],\tag{20}$$

where $\hat{\boldsymbol{x}}$, $\hat{\boldsymbol{y}}$, and $\hat{\boldsymbol{z}}$ are the unit vectors in x, y, and z directions, respectively. Note that the appearance of the imaginary unit in the expression of force is due to the complex form of the spherical harmonics in Eq. (12) and, as a result, the coefficients p_{mn} are also complex numbers. However, the physical quantities like force $\boldsymbol{F}$ in Eq. (20) as well as torque and stresslet in the following remain real. From Eq. (12), the force on the sphere translating with the velocity U in z direction is

$$\boldsymbol{F}=6\pi\mu a\Gamma_{2,3}U\hat{\boldsymbol{z}}.\tag{21}$$

Substituting the solutions in Eqs. (15), (16), and (17) into (9), the velocity field generated by the translating sphere is obtained as

$$\boldsymbol{u}-\boldsymbol{u}^{\infty}=\frac{1}{8\pi\mu}\left(1+\Gamma_{0,2}\frac{a^2}{6}\nabla^2\right)\boldsymbol{J}\cdot\boldsymbol{F},\tag{22}$$

where $\boldsymbol{J}$ is the Oseen-Burgers tensor:

$$J_{ij}(\boldsymbol{r})=\frac{1}{r}\left(\delta_{ij}+\frac{r_i r_j}{r^2}\right).\tag{23}$$

This solution is identical to that in literature.[32,33]

For rotating sphere with the angular velocity $\boldsymbol{\Omega}=(0,0,\Omega)$ we have

$$p_{mn}=\nu_{mn}=0,\tag{24}$$

$$q_{mn}=a\Omega\Gamma_{0,3}\delta_{m0}\delta_{n1}.\tag{25}$$

The torque acting on the particle is given by the coefficients q_{mn} as[12,37]

$$\boldsymbol{T}=8\pi\mu a^2\left[q_{01}\hat{\boldsymbol{z}}-q_{11}\left(\hat{\boldsymbol{x}}+\mathrm{i}\hat{\boldsymbol{y}}\right)\right].\tag{26}$$

Therefore, the torque on the sphere rotating with the angular velocity Ω in z direction is

$$\boldsymbol{T}=8\pi\mu a^3\Gamma_{0,3}\Omega\hat{\boldsymbol{z}}.\tag{27}$$

This agrees with the results by Felderhof[33] and Padmavathi *et al.*[43] Note that the torque $\boldsymbol{T}$ would vanish for the sphere with the perfect-slip surface (for $\widehat{\gamma}=\infty$). The velocity field is then given by

$$\boldsymbol{u}-\boldsymbol{u}^{\infty}=\frac{1}{8\pi\mu}\boldsymbol{R}\cdot\boldsymbol{T},\tag{28}$$

where

$$R_{ij}(\boldsymbol{r}) = \epsilon_{ijk}\frac{r_k}{r^3} = \frac{1}{4}\epsilon_{lkj}\left(\nabla_k J_{il} - \nabla_l J_{ik}\right), \tag{29}$$

and ϵ_{ijk} is the Levi-Civita alternating tensor, that is, $\epsilon_{ijk} = 1$ for $(i, j, k) = (x, y, z)$ and its even permutations, -1 for the odd permutations, and 0 otherwise.

For a sphere in a linear flow with the rate-of-strain tensor given by

$$-E^{\infty}_{ij} = E\left(\hat{z}_i\hat{z}_j - \frac{1}{3}\delta_{ij}\right), \tag{30}$$

we have

$$p_{mn} = \frac{10}{3}aE\Gamma_{2,5}\delta_{m0}\delta_{n2}, \tag{31}$$

$$v_{mn} = \frac{1}{3}aE\Gamma_{0,5}\delta_{m0}\delta_{n2}, \tag{32}$$

$$q_{mn} = 0. \tag{33}$$

The stresslet on the particle is given by the coefficients p_{mn} as[12,44]

$$\begin{aligned}\boldsymbol{S} = 2\pi\mu a^2\Big\{ & p_{02}\left(\hat{\boldsymbol{z}}\hat{\boldsymbol{z}} - \frac{1}{3}\boldsymbol{I}\right) \\ & -p_{12}\left[\hat{\boldsymbol{x}}\hat{\boldsymbol{z}} + \hat{\boldsymbol{z}}\hat{\boldsymbol{x}} + \mathrm{i}\left(\hat{\boldsymbol{y}}\hat{\boldsymbol{z}} + \hat{\boldsymbol{z}}\hat{\boldsymbol{y}}\right)\right] \\ & +2p_{22}\left[\hat{\boldsymbol{x}}\hat{\boldsymbol{x}} - \hat{\boldsymbol{y}}\hat{\boldsymbol{y}} + \mathrm{i}\left(\hat{\boldsymbol{x}}\hat{\boldsymbol{y}} + \hat{\boldsymbol{y}}\hat{\boldsymbol{x}}\right)\right]\Big\}.\end{aligned} \tag{34}$$

Therefore, the stresslet on the sphere in the shear flow with the parameter E is

$$\boldsymbol{S} = \frac{20}{3}\pi\mu a^3\Gamma_{2,5}E\left(\hat{\boldsymbol{z}}\hat{\boldsymbol{z}} - \frac{1}{3}\boldsymbol{I}\right). \tag{35}$$

The velocity field generated by a sphere in a shear flow is given by

$$\boldsymbol{u} - \boldsymbol{u}^{\infty} = -\frac{1}{8\pi\mu}\left(1 + \Gamma_{0,2}\frac{a^2\nabla^2}{10}\right)\boldsymbol{K} : \boldsymbol{S}, \tag{36}$$

where

$$K_{ijk}(\boldsymbol{r}) = -3\frac{r_i r_j r_k}{r^5}. \tag{37}$$

Note that $\boldsymbol{K}$ is always multiplied with the second-rank tensor of symmetric and traceless, and it can be written by the derivative of $\boldsymbol{J}$ as

$$K_{ijk} = \frac{1}{2}\left(\nabla_k J_{ij} + \nabla_j J_{ik}\right). \tag{38}$$

C. Far-Field Effect

From the solution for a single sphere with slip surface expressed by Lamb's general solution, we have the velocity field exerted by a particle at $\boldsymbol{x}_0$ with the force $\boldsymbol{F}$, torque $\boldsymbol{T}$, and stresslet $\boldsymbol{S}$ as

$$\begin{aligned}\boldsymbol{u}(\boldsymbol{x}) - \boldsymbol{u}^{\infty}(\boldsymbol{x}) = \frac{1}{8\pi\mu}\Bigg[& \left(1 + \Gamma_{0,2}\frac{a^2}{6}\nabla^2\right)\boldsymbol{J}(\boldsymbol{x} - \boldsymbol{x}_0)\cdot\boldsymbol{F} \\ & +\boldsymbol{R}(\boldsymbol{x} - \boldsymbol{x}_0)\cdot\boldsymbol{T} - \left(1 + \Gamma_{0,2}\frac{a^2\nabla^2}{10}\right)\boldsymbol{K}(\boldsymbol{x} - \boldsymbol{x}_0) : \boldsymbol{S}\Bigg],\end{aligned} \tag{39}$$

where $\boldsymbol{J}$, $\boldsymbol{R}$, and $\boldsymbol{K}$ are given by Eqs. (23), (29), and (37), respectively. Similar to the no-slip case,[17] this is in the form of multipole expansion by the force moments. Note that this is exact only for the single body problem, but for general situations like many-body problems, it is valid only for the far field where the contribution of the higher force moments (than $\boldsymbol{F}$, $\boldsymbol{T}$, and $\boldsymbol{S}$) are negligible. Here, we define the levels of the truncation, F, FT, and FTS versions: In F version, we only take $\boldsymbol{F}$, in FT version, we take up to $\boldsymbol{T}$, and in FTS version, we take up to $\boldsymbol{S}$.

From the expression, we also obtain Faxén's laws for the slip particle as

$$\boldsymbol{F} = 6\pi\mu a\Gamma_{2,3}\left[\boldsymbol{U} - \boldsymbol{u}^{\infty} - \left(1 + \Gamma_{0,2}\frac{a^2}{6}\nabla^2\right)\boldsymbol{u}'(\boldsymbol{x}_0)\right], \tag{40}$$

$$\boldsymbol{T} = 8\pi\mu a^3\Gamma_{0,3}\left[\boldsymbol{\Omega} - \boldsymbol{\Omega}^{\infty} - \frac{1}{2}\boldsymbol{\nabla}\times\boldsymbol{u}'(\boldsymbol{x}_0)\right], \tag{41}$$

$$\begin{aligned}\boldsymbol{S} = \frac{20}{3}\pi\mu a^3\Gamma_{2,5}\Big\{ & \boldsymbol{0} - \boldsymbol{E}^{\infty} \\ & -\left(1 + \Gamma_{0,2}\frac{a^2\nabla^2}{10}\right)\frac{1}{2}\left[\boldsymbol{\nabla}\boldsymbol{u}' + (\boldsymbol{\nabla}\boldsymbol{u}')^{\dagger}\right](\boldsymbol{x}_0)\Big\},\end{aligned} \tag{42}$$

where $\boldsymbol{u}'$ is the undisturbed velocity field. From these expressions, we can construct the mobility equation

$$\begin{pmatrix}\boldsymbol{U} - \boldsymbol{u}^{\infty} \\ \boldsymbol{\Omega} - \boldsymbol{\Omega}^{\infty} \\ \boldsymbol{0} - \boldsymbol{E}^{\infty}\end{pmatrix} = \begin{pmatrix}\boldsymbol{a} & \widetilde{\boldsymbol{b}} & \widetilde{\boldsymbol{g}} \\ \boldsymbol{b} & \boldsymbol{c} & \widetilde{\boldsymbol{h}} \\ \boldsymbol{g} & \boldsymbol{h} & \boldsymbol{m}\end{pmatrix}\cdot\begin{pmatrix}\boldsymbol{F} \\ \boldsymbol{T} \\ \boldsymbol{S}\end{pmatrix}, \tag{43}$$

where each element in the vectors $(\boldsymbol{U} - \boldsymbol{u}^{\infty}, \boldsymbol{\Omega} - \boldsymbol{\Omega}^{\infty}, \boldsymbol{0} - \boldsymbol{E}^{\infty})$ and $(\boldsymbol{F}, \boldsymbol{T}, \boldsymbol{S})$ contains the quantities for all particles in the system. That is, for N-particle system, $\boldsymbol{F}$ and $\boldsymbol{T}$ have $3N$ elements and $\boldsymbol{S}$ has $5N$ (in reduced form, because S_{ij} is symmetric and traceless). When we write the element explicitly, Greek letters α and β are used for the particle and Roman letters i, j, and k are for the spacial indices x, y, and z. Note that each submatrix in Eq. (43) has different dimension. In the following, we scale the submatrices for (α,β) interaction by $6\pi\mu(a_\alpha)^n$ with $n = 1$ for $\boldsymbol{a}$, $n = 2$ for $\boldsymbol{b}$, $\widetilde{\boldsymbol{b}}$, $\boldsymbol{g}$, and $\widetilde{\boldsymbol{g}}$, and $n = 3$ for the others, and therefore, all matrices are dimensionless. This nondimensionalization reduces to that in conventional Stokesian dynamics[17,18] for monodisperse case. As shown later, $\widetilde{\boldsymbol{b}}$, $\widetilde{\boldsymbol{g}}$, and $\widetilde{\boldsymbol{h}}$ are related to the counterparts $\boldsymbol{b}$, $\boldsymbol{g}$, and $\boldsymbol{h}$, respectively.

From the symmetry of the problem, the submatrices in Eq.

(43) can be written by scalar functions as[17]

$$
\begin{aligned}
a_{ij}^{\alpha\beta} &= x_{\alpha\beta}^{a} e_i e_j + y_{\alpha\beta}^{a}\left(\delta_{ij} - e_i e_j\right), && (44)\\
b_{ij}^{\alpha\beta} &= y_{\alpha\beta}^{b} \epsilon_{ijk} e_k, && (45)\\
c_{ij}^{\alpha\beta} &= x_{\alpha\beta}^{c} e_i e_j + y_{\alpha\beta}^{c}\left(\delta_{ij} - e_i e_j\right), && (46)\\
g_{ijk}^{\alpha\beta} &= x_{\alpha\beta}^{g}\left(e_i e_j - \frac{1}{3}\delta_{ij}\right) e_k \\
&\quad + y_{\alpha\beta}^{g}\left(e_i \delta_{jk} + e_j \delta_{ik} - 2 e_i e_j e_k\right), && (47)\\
h_{ijk}^{\alpha\beta} &= y_{\alpha\beta}^{h}\left(e_i \epsilon_{jkl} e_l + e_j \epsilon_{ikl} e_l\right), && (48)\\
m_{ijkl}^{\alpha\beta} &= \frac{3}{2} x_{\alpha\beta}^{m}\left(e_i e_j - \frac{\delta_{ij}}{3}\right)\left(e_k e_l - \frac{\delta_{kl}}{3}\right) \\
&\quad + \frac{y_{\alpha\beta}^{m}}{2}\left(e_i \delta_{jl} e_k + e_j \delta_{il} e_k + e_i \delta_{jk} e_l + e_j \delta_{ik} e_l \right.\\
&\quad \left. - 4 e_i e_j e_k e_l\right) \\
&\quad + \frac{z_{\alpha\beta}^{m}}{2}\left(\delta_{ik}\delta_{jl} + \delta_{jk}\delta_{il} - \delta_{ij}\delta_{kl} \right.\\
&\quad + e_i e_j \delta_{kl} + \delta_{ij} e_k e_l + e_i e_j e_k e_l \\
&\quad \left. - e_i \delta_{jl} e_k - e_j \delta_{il} e_k - e_i \delta_{jk} e_l - e_j \delta_{ik} e_l\right), && (49)
\end{aligned}
$$

where $\boldsymbol{e} = \boldsymbol{r}/|\boldsymbol{r}|$ is the unit vector of the center-to-center vector $\boldsymbol{r} = \boldsymbol{x}^{(\beta)} - \boldsymbol{x}^{(\alpha)}$. For the self part ($\alpha = \beta$),

$$
\begin{aligned}
x_{11}^{a} = y_{11}^{a} &= \Gamma_{3,2}^{(1)}, && (50)\\
x_{11}^{c} = y_{11}^{c} &= \frac{3}{4}\Gamma_{3,0}^{(1)}, && (51)\\
x_{11}^{m} = y_{11}^{m} = z_{11}^{m} &= \frac{9}{10}\Gamma_{5,2}^{(1)}, && (52)
\end{aligned}
$$

and the others are zero, where the slip factor $\Gamma_{m,n}^{(\alpha)}$ for particle α is defined by

$$
\Gamma_{m,n}^{(\alpha)} = \frac{a_\alpha + m\gamma_\alpha}{a_\alpha + n\gamma_\alpha}. \qquad (53)
$$

Note that the above expressions as well as those in the following are applicable for the case where the slip lengths (as well as the radii) of particles are different (independently).

For the interaction part ($\alpha \neq \beta$), the submatrices can be written by the derivatives of $\boldsymbol{J}$, $\boldsymbol{R}$, and $\boldsymbol{K}$ as

$$
\begin{aligned}
a_{ij}^{12} &= \frac{3a_1}{4}\left(1 + \frac{\overline{a_1}^2 + \overline{a_2}^2}{6}\nabla^2\right) J_{ij}(\boldsymbol{r}), && (54)\\
b_{ij}^{12} &= -\frac{3a_1^2}{8}\epsilon_{ikl}\nabla_k J_{lj}(\boldsymbol{r}), && (55)\\
c_{ij}^{12} &= \frac{3a_1^3}{8}\epsilon_{ikl}\nabla_k R_{lj}(\boldsymbol{r}), && (56)\\
g_{ijk}^{12} &= -\frac{3a_1^2}{8}\left[1 + \left(\frac{\overline{a_1}^2}{10} + \frac{\overline{a_2}^2}{6}\right)\nabla^2\right] \\
&\quad \times\left\{\nabla_j J_{ik}(\boldsymbol{r}) + \nabla_i J_{jk}(\boldsymbol{r})\right\}, && (57)\\
h_{ijk}^{12} &= \frac{3a_1^3}{8}\left\{\nabla_j R_{ik}(\boldsymbol{r}) + \nabla_i R_{jk}(\boldsymbol{r})\right\}, && (58)\\
m_{ijkl}^{12} &= -\frac{3a_1^3}{8}\left(1 + \frac{\overline{a_1} + \overline{a_2}^2}{10}\nabla^2\right) \\
&\quad \times\left\{\nabla_j K_{ikl}(\boldsymbol{r}) + \nabla_i K_{jkl}(\boldsymbol{r})\right\}, && (59)
\end{aligned}
$$

where $\overline{a_\alpha}$ is defined by

$$
\overline{a_\alpha} = a_\alpha\sqrt{\Gamma_{0,2}^{(\alpha)}}, \qquad (60)
$$

and $\boldsymbol{r} = \boldsymbol{x}^{(2)} - \boldsymbol{x}^{(1)}$. Here, to simplify the expressions, we use some properties such as $\nabla^2\nabla^2\boldsymbol{J} = 0$ and $\nabla^2\boldsymbol{R} = 0$. Note that the minus signs in $\boldsymbol{b}$ and $\boldsymbol{g}$ are due to the oddness property about the vector $\boldsymbol{r}$ for $\boldsymbol{R}$, $\boldsymbol{K}$, and $\boldsymbol{\nabla J}$. The submatrices $\widetilde{\boldsymbol{b}}$, $\widetilde{\boldsymbol{g}}$, and $\widetilde{\boldsymbol{h}}$ are related to the counterparts as

$$
\begin{aligned}
b_{ij}^{12} &= \left(\frac{a_1}{a_2}\right)^2 \widetilde{b}_{ij}^{21}, && (61)\\
g_{ijk}^{12} &= -\left(\frac{a_1}{a_2}\right)^2 \widetilde{g}_{kij}^{21}, && (62)\\
h_{ijk}^{12} &= \left(\frac{a_1}{a_2}\right)^3 \widetilde{h}_{kij}^{21}. && (63)
\end{aligned}
$$

After some calculations, we obtain the scalar functions as

$$x_{12}^a = \frac{3a_1}{2r} - \left(\overline{a_1}^2 + \overline{a_2}^2\right)\frac{a_1}{2r^3}, \quad (64)$$

$$y_{12}^a = \frac{3a_1}{4r} + \left(\overline{a_1}^2 + \overline{a_2}^2\right)\frac{a_1}{4r^3}, \quad (65)$$

$$y_{12}^b = -\frac{3a_1^2}{4r^2}, \quad (66)$$

$$x_{12}^c = \frac{3a_1^3}{4r^3}, \quad (67)$$

$$y_{12}^c = -\frac{3a_1^3}{8r^3}, \quad (68)$$

$$x_{12}^g = \frac{9a_1^2}{4r^2} - \left(\frac{\overline{a_1}^2}{10} + \frac{\overline{a_2}^2}{6}\right)\frac{27a_1^2}{2r^4}, \quad (69)$$

$$y_{12}^g = \left(\frac{\overline{a_1}^2}{10} + \frac{\overline{a_2}^2}{6}\right)\frac{9a_1^2}{2r^4}, \quad (70)$$

$$y_{12}^h = -\frac{9a_1^3}{8r^3}, \quad (71)$$

$$x_{12}^m = -\frac{9a_1^3}{2r^3} + \left(\overline{a_1}^2 + \overline{a_2}^2\right)\frac{27a_1^3}{5r^5}, \quad (72)$$

$$y_{12}^m = \frac{9a_1^3}{4r^3} - \left(\overline{a_1}^2 + \overline{a_2}^2\right)\frac{18a_1^3}{5r^5}, \quad (73)$$

$$z_{12}^m = \left(\overline{a_1}^2 + \overline{a_2}^2\right)\frac{9a_1^3}{10r^5}. \quad (74)$$

For no-slip equal spheres ($\overline{a_1} = \overline{a_2} = a$), these reduce to the results by Durlofsky *et al.*[17]

D. Ewald Summation

In the theory above, we can handle many particles in unbounded fluid. However, we may want to introduce periodic boundary conditions, so as to model some sort of systems like dispersions and porous media.

Under the periodic boundary condition, in the FTS version, we have to take into account the periodic images as

$$\begin{pmatrix} \boldsymbol{U}^{(\alpha)} - \boldsymbol{u}^{\infty} \\ \boldsymbol{\Omega}^{(\alpha)} - \boldsymbol{\Omega}^{\infty} \\ \boldsymbol{0} - \boldsymbol{E}^{\infty} \end{pmatrix} = \begin{pmatrix} \boldsymbol{a}^{(\alpha\alpha)} \cdot \boldsymbol{F}^{(\alpha)} \\ \boldsymbol{c}^{(\alpha\alpha)} \cdot \boldsymbol{T}^{(\alpha)} \\ \boldsymbol{m}^{(\alpha\alpha)} \cdot \boldsymbol{S}^{(\alpha)} \end{pmatrix} + \sum_{\gamma}\sum_{\beta}{}' \begin{pmatrix} \boldsymbol{a}^{(\alpha\beta)} & \widetilde{\boldsymbol{b}}^{(\alpha\beta)} & \widetilde{\boldsymbol{g}}^{(\alpha\beta)} \\ \boldsymbol{b}^{(\alpha\beta)} & \boldsymbol{c}^{(\alpha\beta)} & \widetilde{\boldsymbol{h}}^{(\alpha\beta)} \\ \boldsymbol{g}^{(\alpha\beta)} & \boldsymbol{h}^{(\alpha\beta)} & \boldsymbol{m}^{(\alpha\beta)} \end{pmatrix} (\boldsymbol{x}^{(\alpha)} - \boldsymbol{x}^{(\beta)} + \boldsymbol{r}^{(\gamma)}) \cdot \begin{pmatrix} \boldsymbol{F}^{(\beta)} \\ \boldsymbol{T}^{(\beta)} \\ \boldsymbol{S}^{(\beta)} \end{pmatrix}, \quad (75)$$

where γ is an index (n_x, n_y, n_z) for the lattice vector $\boldsymbol{r}^{(\gamma)}$ defined by

$$\boldsymbol{r}^{(\gamma)} = \left(n_x L_x,\ n_y L_y,\ n_z L_z\right), \quad (76)$$

L_x, L_y, and L_z are the linear dimensions of the cell, and the prime on the summation for the particle β denotes that the self term ($\beta = \alpha$) for the primary cell $\boldsymbol{r}^{(\gamma)} = \boldsymbol{0}$ is excluded. The submatrices $\boldsymbol{a}$, etc. are defined by $\boldsymbol{J}$ as same as before. Because of the long range nature of the interaction, Eq. (75) with the infinite summation is difficult to evaluate. By Ewald summation technique,[18,45,46] we can rewrite the infinite summation for the periodic images by two finite summations in real and reciprocal spaces.

First, we split the Oseen-Burgers tensor $J_{ij}(r)$ into two parts as

$$J_{ij}(\boldsymbol{r}) = J_{ij}^{(1)}(\boldsymbol{r}, \xi) + J_{ij}^{(2)}(\boldsymbol{r}, \xi), \quad (77)$$

where

$$J_{ij}^{(1)}(\boldsymbol{r}, \xi) = \left(\nabla^2 \delta_{ij} - \nabla_i \nabla_j\right) r\ \mathrm{erfc}(\xi r), \quad (78)$$

$$J_{ij}^{(2)}(\boldsymbol{r}, \xi) = \left(\nabla^2 \delta_{ij} - \nabla_i \nabla_j\right) r\ \mathrm{erf}(\xi r), \quad (79)$$

with the error function $\mathrm{erf}(x)$ and its complementary $\mathrm{erfc}(x)$. Because all submatrices in the mobility matrix in Eq. (43) are given by the derivatives of $\boldsymbol{J}$ through Eqs. (54) to (59) with (29) and (38), the splitting is simply applicable to them. Here ξ is an arbitrary parameter characterizing the division into the real and reciprocal parts. Usually we take the value with which the division is equal where the computational load is minimized. Because of the factor $\mathrm{erfc}(\xi r)$, $\boldsymbol{J}^{(1)}$ and its derivatives decay rapidly for r. Therefore, we can truncate the lattice summation for γ at some point.

The other contributions coming from $\boldsymbol{J}^{(2)}$ are handled in the reciprocal space in $\boldsymbol{k}$ (the Fourier transformed space). First, we rewrite the summation as

$$\begin{aligned} &\sum_{\gamma}\sum_{\beta}{}' \boldsymbol{M}^{(2)}(\boldsymbol{x}^{(\alpha)} - \boldsymbol{x}^{(\beta)} + \boldsymbol{r}^{(\gamma)}) \cdot \begin{pmatrix} \boldsymbol{F}^{(\beta)} \\ \boldsymbol{T}^{(\beta)} \\ \boldsymbol{S}^{(\beta)} \end{pmatrix} \\ &= \sum_{\gamma}\sum_{\beta} \boldsymbol{M}^{(2)}(\boldsymbol{x}^{(\alpha)} - \boldsymbol{x}^{(\beta)} + \boldsymbol{r}^{(\gamma)}) \cdot \begin{pmatrix} \boldsymbol{F}^{(\beta)} \\ \boldsymbol{T}^{(\beta)} \\ \boldsymbol{S}^{(\beta)} \end{pmatrix} \\ &\quad - \boldsymbol{M}^{(2)}(\boldsymbol{r} = \boldsymbol{0}) \cdot \begin{pmatrix} \boldsymbol{F}^{(\alpha)} \\ \boldsymbol{T}^{(\alpha)} \\ \boldsymbol{S}^{(\alpha)} \end{pmatrix}, \end{aligned} \quad (80)$$

where $\boldsymbol{M}^{(2)}(\boldsymbol{r})$ just denotes the whole matrix for (α, β) interaction coming from $\boldsymbol{J}^{(2)}$. The point is that the summation for the particle β in the second line is running for all particles including α, the self contribution. Applying Poisson's sum formula

$$\sum_{n=-\infty}^{\infty} F(nL) = \frac{1}{L}\sum_{m=-\infty}^{\infty}\int_{-\infty}^{\infty} \mathrm{d}y\ F(y) e^{\mathrm{i}2\pi m y/L}, \quad (81)$$

for the three-dimensional lattice summation, we have

$$\begin{aligned} \sum_{\gamma} \boldsymbol{M}^{(2)}(\boldsymbol{r} + \boldsymbol{r}^{(\gamma)}) &= \frac{1}{V}\sum_{\lambda} e^{-\mathrm{i}\boldsymbol{k}^{(\lambda)}\cdot\boldsymbol{r}} \widetilde{\boldsymbol{M}}^{(2)}(\boldsymbol{k}^{(\lambda)}) \\ &= \frac{1}{V}\sum_{\lambda}\Big[\widetilde{\boldsymbol{M}}^{(2)}_{\mathrm{even}}(\boldsymbol{k}^{(\lambda)})\cos(\boldsymbol{k}^{(\lambda)}\cdot\boldsymbol{r}) \\ &\quad - \widetilde{\boldsymbol{M}}^{(2)}_{\mathrm{odd}}(\boldsymbol{k}^{(\lambda)})\sin(\boldsymbol{k}^{(\lambda)}\cdot\boldsymbol{r})\Big], \end{aligned} \quad (82)$$

where $V = L_x L_y L_z$ is the volume of the periodic cell, λ denotes the index (m_x, m_y, m_z) for the wave vector $\boldsymbol{k}^{(\lambda)}$ defined by

$$\boldsymbol{k}^{(\lambda)} = \left(\frac{2\pi m_x}{L_x}, \frac{2\pi m_y}{L_y}, \frac{2\pi m_z}{L_z} \right), \tag{83}$$

and $\widetilde{\boldsymbol{M}}^{(2)}(\boldsymbol{k})$ is the Fourier transform of $\boldsymbol{M}^{(2)}(\boldsymbol{r})$ defined by

$$\begin{aligned} \widetilde{\boldsymbol{M}}^{(2)}(\boldsymbol{k}) &= \int \mathrm{d}\boldsymbol{r}\ \boldsymbol{M}^{(2)}(\boldsymbol{r})\, e^{\mathrm{i}\boldsymbol{k}\cdot\boldsymbol{r}} \\ &= \int \mathrm{d}\boldsymbol{r}\ \left(\boldsymbol{M}^{(2)}_{\text{even}}(\boldsymbol{r}) + \boldsymbol{M}^{(2)}_{\text{odd}}(\boldsymbol{r}) \right) \left(\cos(\boldsymbol{k}\cdot\boldsymbol{r}) + \mathrm{i}\sin(\boldsymbol{k}\cdot\boldsymbol{r}) \right) \\ &= \widetilde{\boldsymbol{M}}^{(2)}_{\text{even}}(\boldsymbol{k}) + (-\mathrm{i})\widetilde{\boldsymbol{M}}^{(2)}_{\text{odd}}(\boldsymbol{k}). \end{aligned} \tag{84}$$

Note that $\boldsymbol{M}^{(2)}_{\text{even}}$ and $\boldsymbol{M}^{(2)}_{\text{odd}}$ denote the even and odd parts of $\boldsymbol{M}^{(2)}$ for $\boldsymbol{r}$.

Once we have the explicit form of $\widetilde{\boldsymbol{M}}^{(2)}(\boldsymbol{k})$, the last term $\boldsymbol{M}^{(2)}(\boldsymbol{r}=\boldsymbol{0})$ can be obtained analytically by

$$\boldsymbol{M}^{(2)}(\boldsymbol{r}=\boldsymbol{0}) = \frac{1}{(2\pi)^3} \int \mathrm{d}\boldsymbol{k}\ \widetilde{\boldsymbol{M}}^{(2)}(\boldsymbol{k}). \tag{85}$$

Therefore, the infinite lattice summation in Eq. (75) can be calculated by

$$\begin{aligned} \begin{pmatrix} \boldsymbol{U}^{(\alpha)} - \boldsymbol{u}^{\infty} \\ \boldsymbol{\Omega}^{(\alpha)} - \boldsymbol{\Omega}^{\infty} \\ \boldsymbol{0} - \boldsymbol{E}^{\infty} \end{pmatrix} &= \begin{pmatrix} \boldsymbol{a}^{(\alpha\alpha)} \cdot \boldsymbol{F}^{(\alpha)} \\ \boldsymbol{c}^{(\alpha\alpha)} \cdot \boldsymbol{T}^{(\alpha)} \\ \boldsymbol{m}^{(\alpha\alpha)} \cdot \boldsymbol{S}^{(\alpha)} \end{pmatrix} \\ &+ \sum_{\gamma} {\sum_{\beta}}' \boldsymbol{M}^{(1)}(\boldsymbol{x}^{(\alpha)} - \boldsymbol{x}^{(\beta)} + \boldsymbol{r}^{(\gamma)}) \cdot \begin{pmatrix} \boldsymbol{F}^{(\beta)} \\ \boldsymbol{T}^{(\beta)} \\ \boldsymbol{S}^{(\beta)} \end{pmatrix} \\ &+ \frac{1}{V} {\sum_{\lambda}}' \sum_{\beta} \left\{ \widetilde{\boldsymbol{M}}^{(2)}_{\text{even}}(\boldsymbol{k}^{(\lambda)}) \cos\left(\boldsymbol{k}^{(\lambda)} \cdot \left(\boldsymbol{x}^{(\alpha)} - \boldsymbol{x}^{(\beta)} \right) \right) \right. \\ &\left. - \widetilde{\boldsymbol{M}}^{(2)}_{\text{odd}}(\boldsymbol{k}^{(\lambda)}) \sin\left(\boldsymbol{k}^{(\lambda)} \cdot \left(\boldsymbol{x}^{(\alpha)} - \boldsymbol{x}^{(\beta)} \right) \right) \right\} \cdot \begin{pmatrix} \boldsymbol{F}^{(\beta)} \\ \boldsymbol{T}^{(\beta)} \\ \boldsymbol{S}^{(\beta)} \end{pmatrix} \\ &- \boldsymbol{M}^{(2)}(\boldsymbol{r}=\boldsymbol{0}) \cdot \begin{pmatrix} \boldsymbol{F}^{(\alpha)} \\ \boldsymbol{T}^{(\alpha)} \\ \boldsymbol{S}^{(\alpha)} \end{pmatrix}, \end{aligned} \tag{86}$$

where the prime on the summation for λ means to exclude the term with $\boldsymbol{k}^{(\lambda)}$, which should be canceled by the corresponding exerted pressure gradient.[18,47] Mathematically this is equivalent to the renormalization by Batchelor.[48]

Here we give the explicit results only for $\boldsymbol{a}$. The derivations and the full solutions in FTS version are given in Appendix B. The matrix in the real space summation is given by

$$a^{(1;\alpha\beta)}_{ij}(\boldsymbol{r}) = A(r,\xi)\,\delta_{ij} + B(r,\xi)\,\frac{r_i r_j}{r^2}, \tag{87}$$

where

$$A(r,\xi) = \frac{3a_\alpha}{4} \left(A_0(r,\xi) + \frac{\overline{a_\alpha}^2 + \overline{a_\beta}^2}{6} A_2(r,\xi) \right), \tag{88}$$

$$B(r,\xi) = \frac{3a_\alpha}{4} \left(B_0(r,\xi) + \frac{\overline{a_\alpha}^2 + \overline{a_\beta}^2}{6} B_2(r,\xi) \right), \tag{89}$$

$$A_0(r,\xi) = \frac{2\xi}{\sqrt{\pi}} \left(-3 + 2\xi^2 r^2 \right) e^{-\frac{k^2}{4\xi^2}} + \frac{\operatorname{erfc}(\xi r)}{r}, \tag{90}$$

$$A_2(r,\xi) = \frac{2\xi}{\sqrt{\pi}} \frac{1}{r^2} \left(2 + 28\xi^2 r^2 - 40\xi^4 r^4 + 8\xi^6 r^6 \right) e^{-\frac{k^2}{4\xi^2}} + 2\frac{\operatorname{erfc}(\xi r)}{r^3}, \tag{91}$$

$$B_0(r,\xi) = \frac{2\xi}{\sqrt{\pi}} \left(1 - 2\xi^2 r^2 \right) e^{-\frac{k^2}{4\xi^2}} + \frac{\operatorname{erfc}(\xi r)}{r}, \tag{92}$$

$$B_2(r,\xi) = \frac{2\xi}{\sqrt{\pi}} \frac{1}{r^2} \left(-6 - 4\xi^2 r^2 + 32\xi^4 r^4 - 8\xi^6 r^6 \right) e^{-\frac{k^2}{4\xi^2}} - 6\frac{\operatorname{erfc}(\xi r)}{r^3}. \tag{93}$$

The matrix in the reciprocal summation is given by

$$\widetilde{a}^{(2;\alpha\beta)}_{ij}(\boldsymbol{k}) = 6\pi a_\alpha \left(1 - \frac{\overline{a_\alpha}^2 + \overline{a_\beta}^2}{6} k^2 \right) \left(\delta_{ij} - \frac{k_i k_j}{k^2} \right) \times \frac{1}{k^2} \left(1 + \frac{k^2}{4\xi^2} + \frac{k^4}{8\xi^4} \right) \exp\left(-\frac{k^2}{4\xi^2} \right), \tag{94}$$

and the self part is

$$a^{(2;\alpha\beta)}_{ij}(\boldsymbol{r}=\boldsymbol{0}) = \delta_{ij} \frac{a_\alpha \xi}{\sqrt{\pi}} \left[6 - \frac{20}{3} \left(\overline{a_\alpha}^2 + \overline{a_\beta}^2 \right) \xi^2 \right]. \tag{95}$$

III. RESULTS AND DISCUSSIONS

In this section, we present numerical results obtained by the Stokesian dynamics method for the slip particles developed in the previous section under both open and periodic boundary conditions.

A. Open Boundary

For the first example of the numerical solution for slip particles, we study equal-sized particles aligned in the horizontal line. For no-slip particles, Durlofsky *et al.*[17] showed the results for a demonstration of Stokesian dynamics. In the configuration, the translational and angular velocities are solved with a constant force in the perpendicular direction to the alignment.

1. Drag Coefficient

First, we study the translational velocity. In literature, for a particle α with the velocity $U^{(\alpha)}$ under the applied force F, the drag coefficient defined by

$$\widehat{F}(\alpha) = \frac{F}{6\pi\mu a U^{(\alpha)}}, \tag{96}$$

is used to study the falling velocity. Figures 1 and 2 show results of the no-slip and large slip ($\widehat{\gamma} = 100$) cases for various parameters, the number of particles N and the particle distance

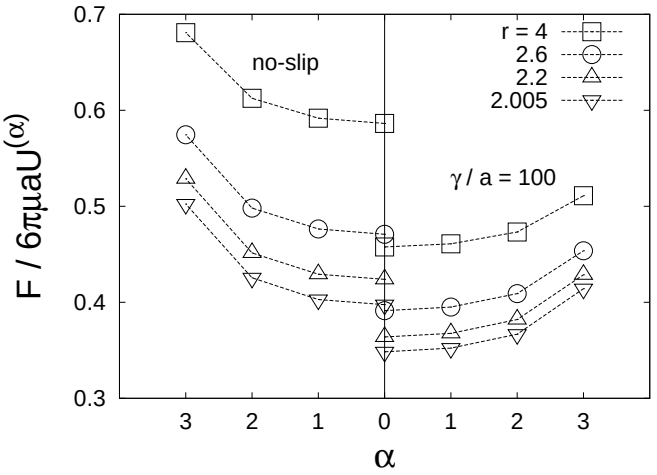

FIG. 1: Drag coefficient $F/6\pi\mu aU^{(\alpha)}$ for horizontally aligned particles with $N = 7$. Here the particle distances are $r = 4$, 2.6, 2.2, and 2.005. The parameter α is the particle index counting from the center with 0 to the edge of the configuration. In the left side, the results for the no-slip particles are shown, while in the right side, those for the slip particles with $\widehat{\gamma} = 100$ are shown. Lines are added for eye guide.

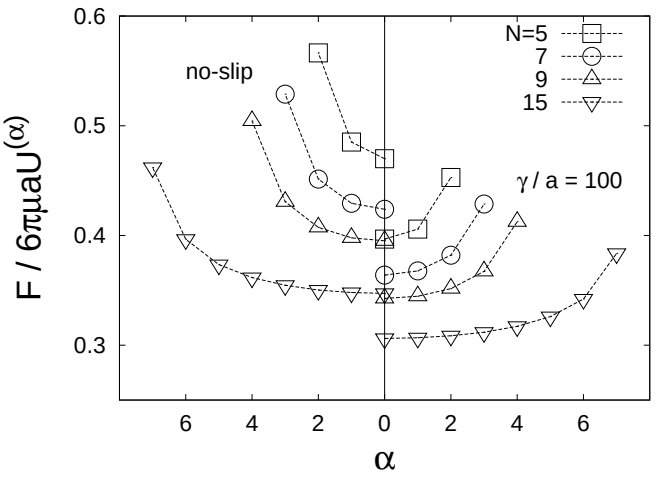

FIG. 2: Drag coefficient $F/6\pi\mu aU^{(\alpha)}$ for horizontally aligned particles with the particle distance $r = 2.2$ and $N = 5$, 7, 9, and 15. In the left side, the results for the no-slip particles are shown, while in the right side, those for the slip particles with $\widehat{\gamma} = 100$ are shown, respectively.

r. From the symmetry, the results are the same with respect to the center particle, so that we plot the half of the system from the center. The results for the no-slip particles agree with those by Durlofsky *et al.*[17] (with their results without lubrication). From the comparison between the no-slip and the slip cases, it is found that the drag coefficients are reduced for the slip particles, while the qualitative behavior looks similar: The center particle falls faster than the particles near the edge, the average velocity for larger system (with larger N) is faster than the smaller system, and the tighter system (with smaller r) is faster than the wider system.

To see more details, let us focus on the system with $N = 7$ and $r = 2.2$. Figure 3 shows the slip-length dependence of the drag coefficient $\widehat{F}$. It is found that, for each particle α, $\widehat{F}$ has two asymptotic values in the no-slip and perfect-slip limits and decreases monotonically as $\widehat{\gamma}$ increases. This corresponds to that fact for a single slip particle in Eq. (21) that the Stokes' drag force $F(\gamma)$ is proportional to $\Gamma_{2,3}$, and for a constant force, the particle falls with the velocity

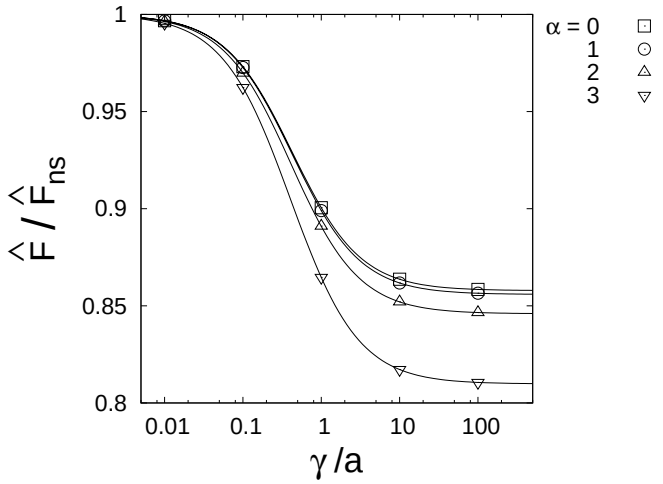

FIG. 3: Drag coefficient $\widehat{F}$ scaled by the no-slip coefficient $\widehat{F}_{\rm ns}$ versus the slip length $\widehat{\gamma}$ for the system with $N = 7$ and $r = 2.2$.

$$U(\gamma) = U_0\Gamma_{3,2}. \tag{97}$$

This means that the particle with the perfect-slip surface falls 3/2 times faster than that with the no-slip surface.

TABLE I: Fitting parameters m and n in Eq. (98) for the system with $N = 7$ and $r = 2.2$.

α	m	n
0	2.0002 ± 0.0001	2.3317 ± 0.0002
1	2.0036 ± 0.0006	2.3410 ± 0.0006
2	2.0510 ± 0.0070	2.4250 ± 0.0080
3	1.9998 ± 0.0001	2.4695 ± 0.0001

Here we try to fit the γ-dependence of $\widehat{F}$ scaled by the no-slip coefficient $\widehat{F}_{\rm ns}$ as

$$\frac{\widehat{F}(\alpha,\widehat{\gamma})}{\widehat{F}_{\rm ns}(\alpha)} = \Gamma_{m,n}, \tag{98}$$

where $\widehat{F}_{\rm ns}(\alpha) = \widehat{F}(\alpha,\widehat{\gamma} = 0)$. The results of the fitting parameters m and n are given in Table I. The lines in Fig. 3 are the fitting results with these m and n. It is found that m is almost constant and close to 2, while n depends on the particle index α. Also we note from Fig. 3 that the slip length $\widehat{\gamma} = 100$ is almost in the asymptotic region in the perfect-slip limit. Therefore, the reduction of the drag coefficient due to the slip surface in the prefect-slip limit is roughly given by the ratio of $\widehat{F}$ at $\widehat{\gamma} = 100$ to the no-slip case, which can be seen in

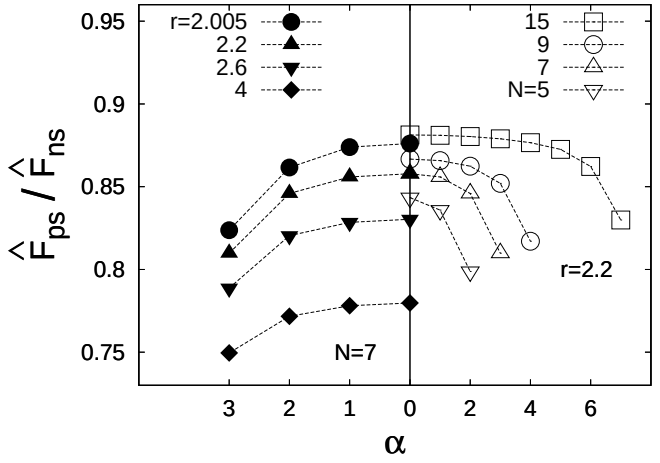

FIG. 4: The drag-reduction rate $\widehat{F}_{\rm ps}/\widehat{F}_{\rm ns}$. The results for the systems with $N = 7$ for various particle distance r are plotted in the left, and those $r = 2.2$ for various N are in the right.

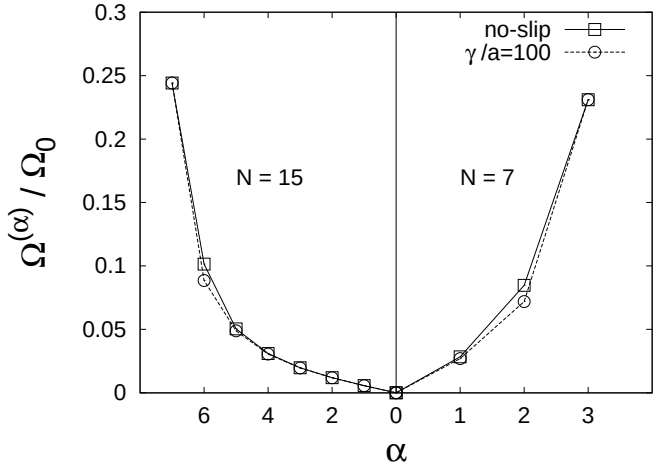

FIG. 5: Angular velocities $\Omega^{(\alpha)}$ divided by $\Omega_0 = T/8\pi\mu a^3$ for the systems of $N = 15$ (on the left side) and 7 (on the right side) with the same particle distance $r = 2.2$. The results are given for the no-slip case and large slip-length case ($\widehat{\gamma} = 100$).

Figs. 1 and 2: The change from the left (no-slip) to the right ($\widehat{\gamma} = 100$) is the drag reduction due to the surface slip.

The drag-reduction rate from the no-slip to perfect-slip conditions $\widehat{F}_{\rm ps}/\widehat{F}_{\rm ns}$ can be estimated by the fitting parameters as

$$\frac{\widehat{F}_{\rm ps}}{\widehat{F}_{\rm ns}} = \frac{m}{n}, \tag{99}$$

where $\widehat{F}_{\rm ps} = \widehat{F}(\widehat{\gamma} = \infty)$. This is because the asymptotic value of $\Gamma_{m,n}$ is equal to m/n. Figure 4 shows the drag-reduction rates for the various cases. It is found that the sparse configuration (lager r) has bigger reduction, the smaller system (smaller N) has bigger reduction, and the edge (center) particle always has the biggest (smallest) reduction in the system. Here we calculated the systems up to $N = 15$, but the qualitatively similar behavior would be obtain for larger system, where main portion has nearly same velocity and a few particles near the edges have the smaller one.

2. *Angular Velocity*

Next, we look at the angular velocity. The results for the no-slip case agree with those by Durlofsky *et al.*[17] as for the drag coefficient.

Figure 5 shows the angular velocities $\Omega^{(\alpha)}$ of particle α divided by the single-particle angular velocity $\Omega_0 = T/8\pi\mu a^3$ for two slip lengths, no-slip and large slip ($\widehat{\gamma} = 100$), for the two systems, $N = 15$ and 7, with the same particle distance $r = 2.2$. It is seen that the slip-length dependence is relatively small. The center particle has zero rotation (from the symmetry). The angular velocities of particles from the next to the center to the third from the edge ($\alpha = 5$ for $N = 15$ and $\alpha = 1$ for $N = 7$) has just a slight decrease for the large slip length. The largest influence of the slip length appears on the second particle from the edge for both cases (at $\alpha = 6$ for $N = 15$ and $\alpha = 2$ for $N = 7$). The terminal particles has no $\widehat{\gamma}$-dependence.

One of the reasons why the angular velocity depends very slightly on the slip length could be because in the present situation the particles are torque free and therefore all the γ-dependence on Ω is coming from the disturbance field generated by the external force F on the particles. However, if external torque is applied to the system, it is expected from the single-body solution in Eq. (27) that the γ-dependence on the angular velocity would be large. See Sec. III B 2 in the following for the periodic system.

B. Periodic Boundary

Next, we study the system under the periodic boundary condition. The particle configuration we study is the simple cubic array. The results for no-slip particles are summarized in Brady *et al.*[18] In the following, we see the slip-length dependencies for basic rheological properties, sedimentation velocity, and the spin and shear viscosities, in details.

1. *Sedimentation Velocity*

First, sedimentation velocity is calculated, where a constant force is applied to the particles. Here, we study the velocity U divided by the falling velocity for a single particle $U_0 = F/6\pi\mu a$, where F is the strength of the force. Note that for the regular array configurations, the sedimentation velocity for each particles are the same and, as a result, it is equivalent to the problem of fixed particles under a constant velocity, in other words, a pressure-driven flow in the porous medium.

For no-slip particles in the regular array configurations, there are theoretical and numerical studies. Hasimoto[47] got the sedimentation velocities for the regular arrays where the

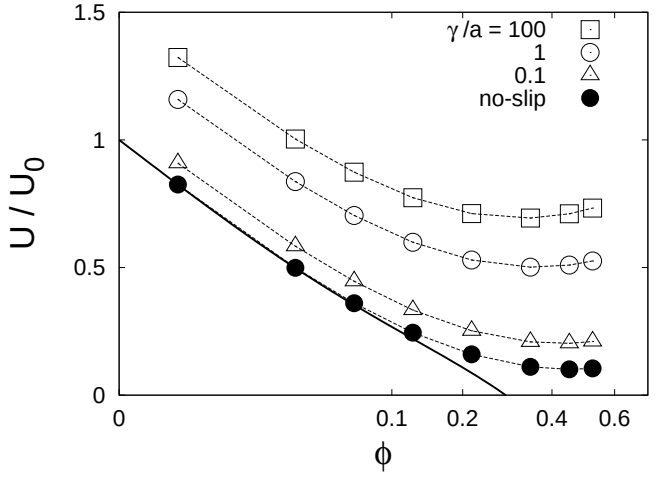

FIG. 6: Sedimentation velocities for various slip length γ divided by $U_0 = F/6\pi\mu a$ versus volume fraction ϕ for the particles in the simple-cubic array configuration. The horizontal axis is not linear but $\phi^{1/3}$. The solid line is the dilute limit for the no-slip particles in Eq. (100) by Hasimoto.[47]

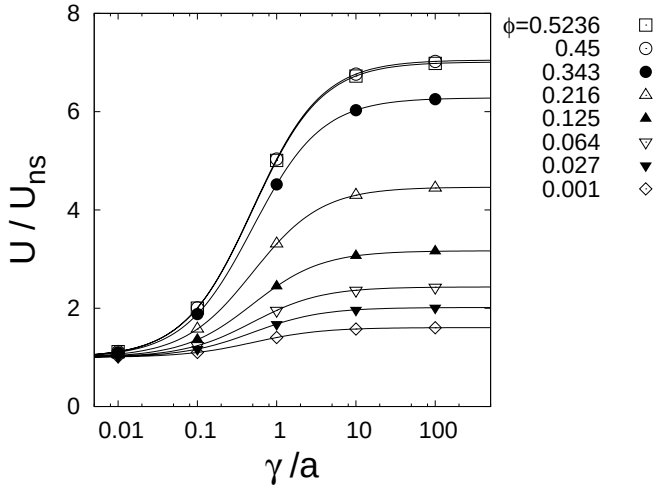

FIG. 7: The scaled sedimentation velocities $U/U_{\rm ns}$ versus the scaled slip length $\widehat{\gamma}$, where $U_{\rm ns}$ is the sedimentation velocity for the no-slip case $\widehat{\gamma} = 0$.

dilute limit form for the simple-cubic array was given by

$$\frac{U(\phi,\widehat{\gamma}=0)}{U_0} = 1 - 1.7601\phi^{1/3} + \phi - 1.5593\phi^2. \qquad (100)$$

Zick and Homsy[49] and Brady *et al.*[18] showed the numerical calculations.

Here, calculations for the slip particles including no-slip case are done by the method in the FTS version formulated in the previous section (so that lubrication as well as effective quadrupole contribution in Brady *et al.*[18] are not included). The periodic cell contains 8 particles of equal size. Figure 6 and Table II show U/U_0 for the slip lengths $\widehat{\gamma} = 0$, 0.01, 0.1, 1, 10, and 100. The no-slip results agree with the dilute limit theory in Eq. (100) by Hasimoto[47] and the corresponding results by Brady *et al.*[18] (for $\langle M^*_{UF}\rangle$ in their notation). The results for the finite slip lengths show that as the slip length increases, the sedimentation velocity also increases. In other words, the particles with larger slip length have less friction. Figure 7 shows the slip-length dependence on the scaled sedimentation velocity defined by

$$\widehat{U}(\phi,\widehat{\gamma}) = \frac{U(\phi,\widehat{\gamma})}{U_{\rm ns}(\phi)}, \qquad (101)$$

where $U_{\rm ns}(\phi) = U(\phi,\widehat{\gamma}=0)$. From the results, $\widehat{U}$ has two asymptotes in $\gamma \to 0$ and $\gamma \to \infty$. Therefore, we try to fit the slip-length dependence as

$$\widehat{U}(\phi,\widehat{\gamma}) = \Gamma_{m,n}, \qquad (102)$$

where m and n are the fitting parameters depending on the volume fraction ϕ. The results for m and n by the least-square fitting for each ϕ are summarized in Table III. We find that n is not dependent of ϕ, and actually $n = 2$ with the error less than 0.5%. The other parameter m is almost linearly increasing for ϕ except for the dense region. Note that in the dilute limit ($\phi \to 0$), from the single-body solution in Eq. (21), it is expected that $\widehat{U} \to \Gamma_{3,2}$. Here, we assume the ϕ-dependence of m in the form $m(\phi) = 3 + A\phi$. By the least-square fitting for the range $0 \le \phi < 0.4$, we have $A = 27.9 \pm 0.4$. That is, the scaled sedimentation velocity is approximately given by

$$\widehat{U}(\phi,\widehat{\gamma}) = \frac{1 + (3 + A\phi)\widehat{\gamma}}{1 + 2\widehat{\gamma}}. \qquad (103)$$

Note that, from Eq. (102), the asymptotic value in the perfect-slip limit of $\widehat{U}$ is m/n, which is the ratio of the mobilities of the perfect-slip to the no-slip. It is an increasing function of ϕ from 1.5 in the dilute limit to roughly 7 in the dense case as shown in Fig. 7. As mentioned above, the results of sedimentation velocity for the regular array can be interpreted in terms of the permeability of porous medium for fluid flow. This implies that the permeability of the perfect-slip arrays might be 7 times larger than that of the no-slip arrays at most in the low porosity limit. This type of large increase of the permeability would be expected in the nanofluidic devices with the slip surface, although the ratio would depend on the detailed configurations. According to the lack of lubrication effect in the present formulation, the ratio shown above is underestimated, and it would be more than that if the contribution of the higher force moments is taken into account.

2. *Spin Viscosity*

Next, we study the problem with applied torque for the same configuration. The results are shown in Table IV. From the single-body solution in Eq. (27), the angular velocity scaled by $\Omega_0 = T/8\pi\mu a^3$ in the dilute limit becomes

$$\lim_{\phi\to 0} \frac{\Omega(\phi,\widehat{\gamma})}{\Omega_0} = \Gamma_{3,0}. \qquad (104)$$

TABLE II: Sedimentation velocities U/U_0 for various slip length γ in the simple-cubic array configuration.

ϕ	$\widehat{\gamma}=0$	$\widehat{\gamma}=0.01$	$\widehat{\gamma}=0.1$	$\widehat{\gamma}=1$	$\widehat{\gamma}=10$	$\widehat{\gamma}=100$
0.001	0.8250	0.8348	0.9084	1.1585	1.3014	1.3227
0.027	0.4990	0.5089	0.5834	0.8368	0.9816	1.0032
0.064	0.3600	0.3701	0.4460	0.7040	0.8514	0.8734
0.125	0.2449	0.2554	0.3335	0.5991	0.7509	0.7735
0.216	0.1599	0.1708	0.2523	0.5293	0.6875	0.7112
0.343	0.1109	0.1224	0.2085	0.5014	0.6688	0.6938
0.450	0.1012	0.1132	0.2033	0.5095	0.6845	0.7107
0.5236	0.1050	0.1173	0.2101	0.5256	0.7058	0.7327

TABLE III: Fitting parameters m and n in Eq. (102).

ϕ	m		n	
0.001	3.2128	$\pm 3\cdot 10^{-5}$	2.00001	$\pm 2\cdot 10^{-5}$
0.027	4.0313	$\pm 3\cdot 10^{-5}$	2.00004	$\pm 2\cdot 10^{-5}$
0.064	4.86705	$\pm 8\cdot 10^{-6}$	2	$\pm 4\cdot 10^{-6}$
0.125	6.356	± 0.007	2.004	± 0.002
0.216	8.97	± 0.01	2.004	± 0.003
0.343	12.62	± 0.02	2.004	± 0.003
0.45	14.19	± 0.02	2.004	± 0.003
0.5236	14.13	± 0.03	2.006	± 0.004

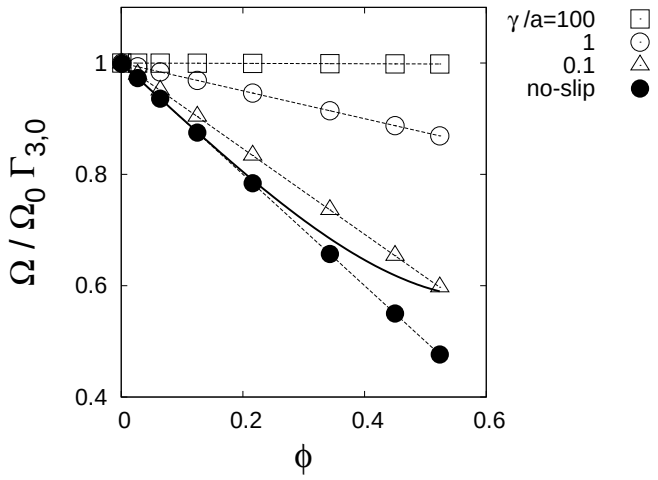

FIG. 8: Angular velocity Ω divided by the factor $\Omega_0\Gamma_{3,0}$, the single slip particle's result, versus volume fraction ϕ for the particles in the simple-cubic array configuration. The solid line is the dilute limit for the no-slip particles derived from Eq. (107) obtain by Zuzovsky *et al.*[50] The dashed lines are fitted by Eq. (112).

That is, the angular velocity is diverging in the perfect-slip limit as seen in Table IV. Figure 8 shows Ω scaled by $\Omega_0\Gamma_{3,0}$. It is observed that for the no-slip case, the angular velocity Ω decays for ϕ, but the ϕ dependence reduces as the slip length increases.

This is a mobility problem. For the regular array configuration, again, it is closely related to the corresponding resistance problem, where the torque is solved under the constant rotation of the particles. The spin viscosity ζ is defined by the ratio of the mean torque to the rotation as

$$\langle T\rangle = -\mu\zeta\langle\Omega\rangle, \tag{105}$$

where $\langle\cdot\rangle$ denotes the bulk average. Therefore, for the present case, $\langle T\rangle = -nT$ and $\langle\Omega\rangle = \Omega$, where n is the number density of particles, and T and Ω are the torque on and angular velocity of each particle, and we obtain the relation

$$\zeta = 6\phi\frac{\Omega_0}{\Omega}. \tag{106}$$

For no-slip particles, Zuzovsky *et al.*[50] gave the dilute limit for the spin viscosity ζ as

$$\zeta = 6\phi\left[1-\phi+12\left(\tilde{a}_{20}\right)^2\phi^{10/3}+O\left(\phi^{14/3}\right)\right]^{-1}, \tag{107}$$

with $\tilde{a}_{20} = 0.2857$ for the simple cubic lattice. The corresponding angular velocity is shown in Fig. 8 by the solid line. From the result, however, the no-slip behavior is rather well represented by the expression without $O(\phi^{10/3})$ term

$$\frac{\Omega_{\rm ns}(\phi)}{\Omega_0} = 1-\phi. \tag{108}$$

This is due to the lack of higher force moments in the present calculations.

To see the slip-length dependence, we define the scaled angular velocity $\widehat{\Omega}$ by

$$\widehat{\Omega}(\phi,\widehat{\gamma}) = \frac{\Omega(\phi,\widehat{\gamma})}{\Omega_{\rm ns}(\phi)}. \tag{109}$$

Figure 9 shows the slip-length dependence of $\widehat{\Omega}$. It is seen that $\widehat{\Omega}$ goes to asymptotes in the perfect-slip limit from unity in the no-slip limit. Therefore, we try to fit $\widehat{\gamma}$ dependence by the form

$$\widehat{\Omega}(\phi,\widehat{\gamma}) = \Gamma_{m,n}. \tag{110}$$

Fitting results for each ϕ are summarized in Table V. It is found again that n is independent of ϕ and $n=3$. For m, it is well represented by

$$m(\phi) = \frac{3}{1-A\phi}, \tag{111}$$

TABLE IV: Angular velocities Ω/Ω_0 in the simple-cubic array configuration.

ϕ	$\widehat{\gamma}=0$	$\widehat{\gamma}=0.01$	$\widehat{\gamma}=0.1$	$\widehat{\gamma}=1$	$\widehat{\gamma}=10$	$\widehat{\gamma}=100$
0.001	0.9990	1.0290	1.2990	3.9990	30.9990	300.9990
0.027	0.9730	1.0030	1.2730	3.9730	30.9730	300.9730
0.064	0.9360	0.9660	1.2360	3.9360	30.9360	300.9360
0.125	0.8750	0.9050	1.1750	3.8750	30.8750	300.8750
0.216	0.7840	0.8140	1.0840	3.7840	30.7840	300.7840
0.343	0.6570	0.6870	0.9570	3.6570	30.6570	300.6570
0.450	0.5500	0.5800	0.8500	3.5500	30.5500	300.5500
0.5236	0.4764	0.5064	0.7764	3.4764	30.4764	300.4764

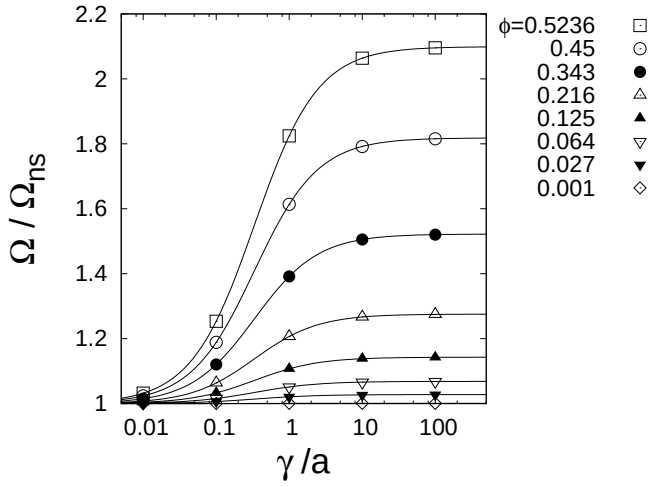

FIG. 9: The scaled angular velocity $\Omega/\Omega_{\rm ns}$ for the simple-cubic configuration, where $\Omega_{\rm ns}$ is the angular velocity for the no-slip case.

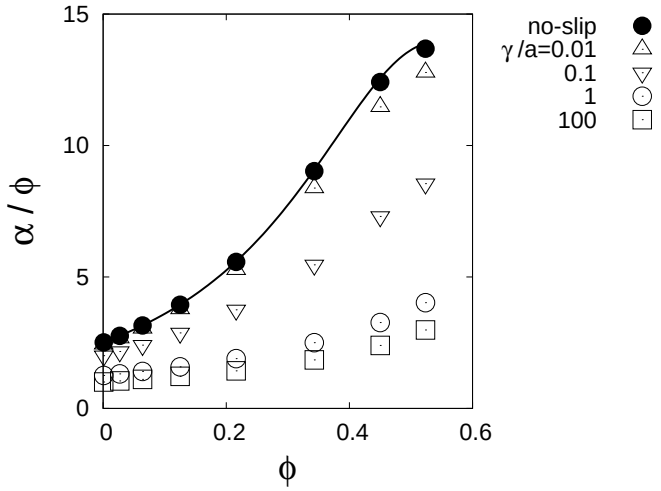

FIG. 10: Viscosity function α divided by ϕ for the simple-cubic configuration. The solid line is obtained from the dilute limit for the no-slip particles in Eq. (115) by Zuzovsky *et al.*[50]

TABLE V: Fitting parameters m and n in Eq. (110). The data for $\phi=0.001$ is fitted only by m with $n=3$.

ϕ	m		n	
0.001	3.003	$\pm4\cdot10^{-7}$	–	–
0.027	3.0834	±0.0001	3.00011	±0.0001
0.064	3.20514	$\pm4\cdot10^{-5}$	3.00002	$\pm4\cdot10^{-5}$
0.125	3.42854	$\pm2\cdot10^{-5}$	2.99997	$\pm1\cdot10^{-5}$
0.216	3.82653	$\pm1\cdot10^{-5}$	3	$\pm1\cdot10^{-5}$
0.343	4.56623	$\pm1\cdot10^{-5}$	3.00001	$\pm7\cdot10^{-6}$
0.450	5.45454	$\pm7\cdot10^{-6}$	3	$\pm4\cdot10^{-6}$
0.5236	6.29724	$\pm2\cdot10^{-5}$	3.00001	$\pm1\cdot10^{-5}$

with $A=1\pm6\times10^{-6}$. Thus, we conclude that the angular velocity $\Omega(\phi,\widehat{\gamma})$ is expressed by

$$\frac{\Omega(\phi,\widehat{\gamma})}{\Omega_0}=\frac{1-\phi+3\widehat{\gamma}}{1+3\widehat{\gamma}}. \tag{112}$$

From the results, it is found that the increase of the scaled angular velocity $\widehat{\Omega}$ from the no-slip limit to the perfect-slip limit, which is the reduction rate of the spin viscosity, is 1 in the dilute limit, but it increases roughly up to twice as the volume fraction ϕ increases.

3. *Shear Viscosity*

The effective viscosity tensor μ^*_{ijkl} relating the bulk stress $\langle\boldsymbol{\sigma}\rangle$ and the bulk rate-of-strain $\langle\boldsymbol{E}\rangle$ is defined by

$$\langle\sigma_{ij}\rangle=2\mu^*_{ijkl}\langle E_{kl}\rangle, \tag{113}$$

where, for a cubic lattice, μ^*_{ijkl} is given by two scalar functions α and β as[50,51]

$$\begin{aligned}\mu^*_{ijkl} &= \mu\big(1+\beta\big)\frac{1}{2}\left(\delta_{ik}\delta_{jl}+\delta_{il}\delta_{jk}-\frac{2}{3}\delta_{ij}\delta_{kl}\right)\\ &\quad+\mu\big(\alpha+\beta\big)\left(\delta_{ijkl}-\frac{1}{3}\delta_{ij}\delta_{kl}\right).\end{aligned} \tag{114}$$

Here, δ_{ijkl} is unity if all the indices are the same and zero otherwise. The bulk stress is given by the stresslet on the particle $\boldsymbol{S}$ as $\langle\boldsymbol{\sigma}\rangle=2\mu\langle\boldsymbol{E}\rangle-n\langle\boldsymbol{S}\rangle$, where the first term is the contribution of the fluid and n is the number density of the particle, so that we can evaluate α and β by solving $\boldsymbol{S}$ under the rate-of-strain $\boldsymbol{E}$. The results are shown in Table VI.

For no-slip particles, Zuzovsky *et al.*[50] gave the dilute limits

TABLE VI: Viscosity functions α and β divided by ϕ in the simple-cubic array configuration.

ϕ	α/ϕ for $\widehat{\gamma}=0$	$\widehat{\gamma}=0.01$	$\widehat{\gamma}=0.1$	$\widehat{\gamma}=1$	$\widehat{\gamma}=10$	$\widehat{\gamma}=100$
0.001	2.5094	2.4375	2.0060	1.2524	1.0310	1.0045
0.027	2.7591	2.6727	2.1644	1.3144	1.0735	1.0449
0.064	3.1537	3.0427	2.4073	1.4078	1.1378	1.1062
0.125	3.9450	3.7787	2.8708	1.5801	1.2571	1.2199
0.216	5.5745	5.2730	3.7515	1.8937	1.4760	1.4289
0.343	9.0255	8.3823	5.4624	2.5007	1.9092	1.8441
0.450	12.4144	11.4696	7.3016	3.2662	2.4822	2.3964
0.5236	13.6821	12.7794	8.5491	4.0221	3.0878	2.9843

ϕ	β/ϕ for $\widehat{\gamma}=0$	$\widehat{\gamma}=0.01$	$\widehat{\gamma}=0.1$	$\widehat{\gamma}=1$	$\widehat{\gamma}=10$	$\widehat{\gamma}=100$
0.001	2.4979	2.4266	1.9987	1.2495	1.0290	1.0026
0.027	2.4567	2.3874	1.9702	1.2359	1.0189	0.9929
0.064	2.4236	2.3550	1.9424	1.2174	1.0033	0.9777
0.125	2.4135	2.3425	1.9191	1.1886	0.9763	0.9509
0.216	2.4809	2.3992	1.9236	1.1492	0.9342	0.9089
0.343	2.7462	2.6304	1.9984	1.0999	0.8751	0.8491
0.450	3.1952	3.0172	2.1277	1.0627	0.8263	0.7998
0.5236	3.7192	3.4569	2.2611	1.0390	0.7938	0.7668

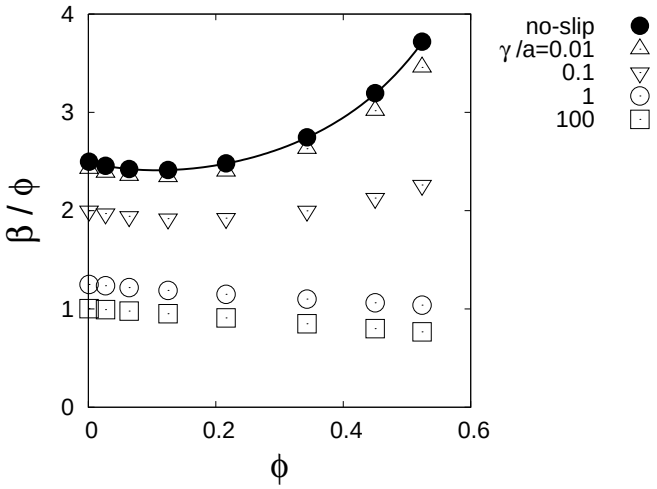

FIG. 11: Viscosity function β divided by ϕ for the simple-cubic configuration. The solid line is obtained from the dilute limit for the no-slip particles in Eq. (116) by Zuzovsky *et al.*[50]

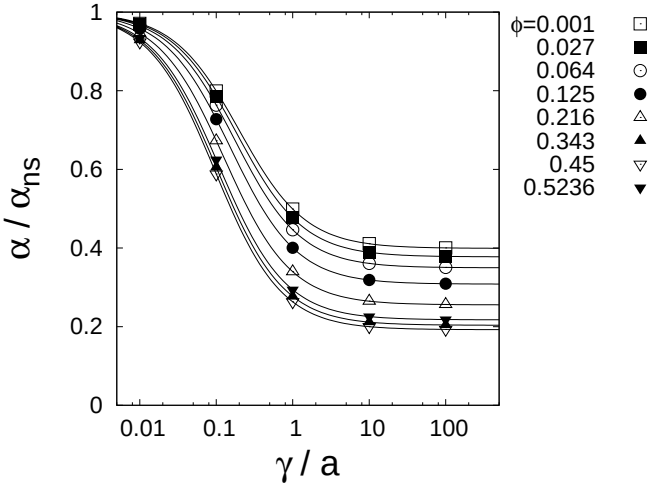

FIG. 12: The scaled viscosity function $\widehat{\alpha}$ versus the scaled slip length $\widehat{\gamma}$ for the simple-cubic configuration.

for $\alpha(\phi)$ and $\beta(\phi)$ as

$$\alpha = \frac{5}{2}\phi\left[1-\left(1-60\tilde{b}_{20}\right)\phi+12\tilde{a}_{20}\phi^{5/3}+O\left(\phi^{7/3}\right)\right]^{-1} \quad (115)$$

$$\beta = \frac{5}{2}\phi\left[1-\left(1+40\tilde{b}_{20}\right)\phi-8\tilde{a}_{20}\phi^{5/3}+O\left(\phi^{7/3}\right)\right]^{-1} \quad (116)$$

where for the simple cubic lattice $\tilde{a}_{20}=0.2857$ and $\tilde{b}_{20}=-0.04655$. Note that $\tilde{a}_{20}$ is the same value for the spin viscosity. Figures 10 and 11 show α/ϕ and β/ϕ for various slip lengths. Because of the lack of lubrication contribution in the present calculations, the diverging behavior of the viscosity in the closed packing limit is not captured. However, for the no-slip case, the agreement of the numerical results with the dilute limit expressions (115) and (116) is very good.

To see the slip-length dependence, we scale the functions by those for the no-slip case as

$$\widehat{\alpha}=\frac{\alpha(\phi,\widehat{\gamma})}{\alpha_{\rm ns}(\phi)}, \quad \widehat{\beta}=\frac{\beta(\phi,\widehat{\gamma})}{\beta_{\rm ns}(\phi)}, \quad (117)$$

where $\alpha_{\rm ns}=\alpha(\phi,\widehat{\gamma}=0)$ and $\beta_{\rm ns}=\beta(\phi,\widehat{\gamma}=0)$. Figures 12 and 13 show the slip-length dependencies of $\widehat{\alpha}$ and $\widehat{\beta}$, respectively. As similar before, we try to fit them by $\Gamma_{m,n}$:

$$\widehat{\alpha}(\phi,\widehat{\gamma})=\Gamma_{m_\alpha,n_\alpha}, \quad \widehat{\beta}(\phi,\widehat{\gamma})=\Gamma_{m_\beta,n_\beta}, \quad (118)$$

where (m_α,n_α), and (m_α,n_α) are the fitting parameters. From the single-body solution (35), the dilute limits for $\widehat{\alpha}$ and $\widehat{\beta}$ should be $\Gamma_{5,2}$, that is, it is expected that $m\to 5$ and $n\to 2$ in the limit $\phi\to 0$ for both $\widehat{\alpha}$ and $\widehat{\beta}$. The results are summarized

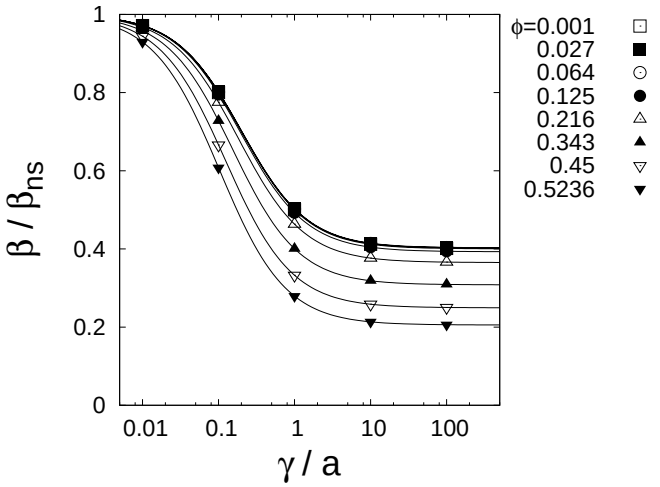

FIG. 13: The scaled viscosity function $\widehat{\beta}$ versus the scaled slip length $\widehat{\gamma}$ for the simple-cubic configuration.

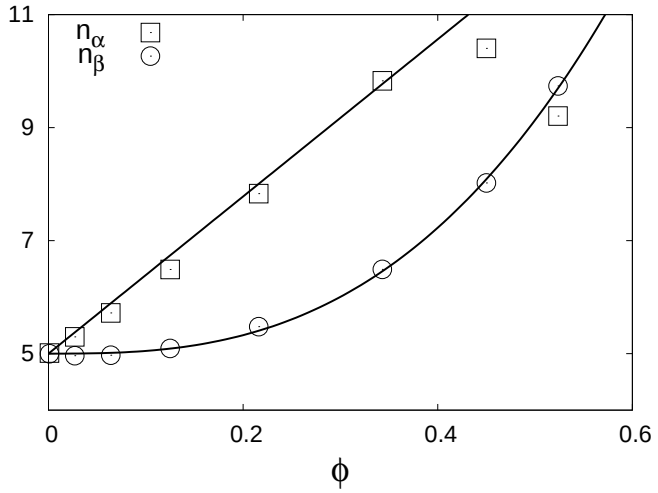

FIG. 14: Fitting parameters $n_\alpha(\phi)$ and $n_\beta(\phi)$. The solid lines are given by Eq. (120).

TABLE VII: Fitting parameters m and n in Eq. (118).

ϕ	m_α	n_α
0.001	$2 \pm 2 \cdot 10^{-5}$	$5.01127 \pm 4 \cdot 10^{-5}$
0.027	$2 \pm 1 \cdot 10^{-5}$	$5.29765 \pm 3 \cdot 10^{-5}$
0.064	$2 \pm 1 \cdot 10^{-5}$	$5.72049 \pm 3 \cdot 10^{-5}$
0.125	$2 \pm 1 \cdot 10^{-5}$	$6.49001 \pm 3 \cdot 10^{-5}$
0.216	$2 \pm 1 \cdot 10^{-5}$	$7.83125 \pm 2 \cdot 10^{-5}$
0.343	$2 \pm 4 \cdot 10^{-6}$	$9.82756 \pm 1 \cdot 10^{-5}$
0.450	$2 \pm 3 \cdot 10^{-5}$	$10.40260 \pm 1 \cdot 10^{-4}$
0.5236	$2 \pm 5 \cdot 10^{-6}$	$9.20504 \pm 2 \cdot 10^{-5}$
ϕ	m_β	n_β
0.001	$2 \pm 3 \cdot 10^{-5}$	$4.99750 \pm 7 \cdot 10^{5}$
0.027	$2 \pm 3 \cdot 10^{-5}$	$4.96357 \pm 6 \cdot 10^{5}$
0.064	$2 \pm 6 \cdot 10^{-6}$	$4.97254 \pm 1 \cdot 10^{5}$
0.125	$2 \pm 2 \cdot 10^{-5}$	$5.09142 \pm 4 \cdot 10^{5}$
0.216	$2 \pm 2 \cdot 10^{-5}$	$5.47661 \pm 4 \cdot 10^{5}$
0.343	$2 \pm 2 \cdot 10^{-5}$	$6.49057 \pm 5 \cdot 10^{5}$
0.450	$2 \pm 1 \cdot 10^{-5}$	$8.02057 \pm 4 \cdot 10^{5}$
0.5236	$2 \pm 1 \cdot 10^{-5}$	$9.73869 \pm 4 \cdot 10^{5}$

in Table VII. At this time, it is found that m is independent of ϕ for $\widehat{\alpha}$ and $\widehat{\beta}$, so that $m = 2$. The other parameters n_α and n_β can be approximated as

$$n_\alpha = 5 + A\phi, \tag{119}$$

$$n_\beta = 5 + B\phi^C, \tag{120}$$

with $A = 13.9 \pm 0.2$, $B = 28 \pm 2$, and $C = 2.8 \pm 0.1$, where, for n_α, two points in dense region ($\phi = 0.45$ and 0.5236) are ignored. The results are given in Fig. 14.

Similar to the drag coefficient and spin viscosity, the shear viscosity has the reduction according to the surface slip. Figures 12 and 13 show that the shear viscosity is reduced to 40% even in the dilute limit and to 20% in the dense case. It should be noted that, in the present calculations, lubrication effect which is dominant in the dense configurations is not included. Therefore, at this stage, we do not know whether the diverging behavior of the shear viscosity (as well as spin viscosity) in the no-slip limit would hold in the finite slip-length case.

IV. CONCLUDING REMARKS

We have formulated hydrodynamic interaction among spherical particles with arbitrary sizes and arbitrary slip length in general linear flows, including constant imposed flow (pressure-driven flow) and shear flows. It has been implemented into the Stokesian dynamics method for both open and periodic boundary conditions, for the latter using Ewald summation technique. We have demonstrated that the formulation is capable of representing the slip boundary condition on the surface of particles properly. We have also calculated basic rheological properties such as sedimentation velocity, spin and shear viscosities for the entire range of the slip length, from the no-slip limit (zero slip length) to the perfect-slip limit (infinite slip length).

From the calculations of particles in unbounded fluid shown in Sec. III A, it is demonstrated that the drag coefficient depends not only on the number of particles and the separation but also on the slip length. This implies that the slip length is one of the important parameters for the mechanism of selection in nanofluidic devices by the difference in the drag coefficients (or equivalently, sedimentation velocity). From the results for regular array configurations in Sec. III B, which is closely related to the flow through porous media, it is found that the drag reduction is enhanced for dense configurations, about 7 times larger than the no-slip limit. For the spin viscosity, i.e., the torque response on the particles by the applied rotation, as expected from the single-body solution, the torque is vanishing in the perfect-slip limit. The volume fraction dependence also reduces to zero in the limit. The reduction of the rotational drag is also enhanced for the dense configurations, but the rate is up to around 2. For the shear viscosity,

the reduction due to the surface slip is also obtained. The viscosity reduces to 40% even in the dilute limit and to 20% in the dense case.

One of the major applications of micro- and nanofluidics is to make a good device to separate a certain type of components (specific DNA or particles with a given size, for example) out of the mixtures. Any effect that depends on the properties of the target like the size or chemical properties can be used. The drag coefficient due to the surrounding fluid, which is discussed in the present article, is one of them. The flows we have studied in this paper, especially for the regular arrays, should reflect major physics occurring in the experiments on nanofluidics for nano-porous media,[52] flows around obstacles in nano channels,[53] and other nanofluidic flows.

The formulation of the hydrodynamic theory and implementation of the numerical scheme in this article is just a first step to establish a theoretical foundation for nanofluidics. To achieve the goal, one direction is a multiple scale approach making a bridge between the present hydrodynamic theory and the molecular theory. We plan several improvements for the hydrodynamic theory presented in this paper: (i) The contribution of higher force moments, which becomes important in dense configurations and close geometries, can be incorporated into the present formulation by using lubrication theory.[16–18] Unfortunately there are no results available at this moment in literature, but we can use the exact solutions for two-body problem in the series expression.[40] (ii) The Brownian force, another important contribution from the fluid to the object in nano scale, can be introduced into the framework of Stokesian dynamics method.[22,54–57] (iii) It is highly demanded to solve the hydrodynamic interaction among the objects of arbitrary shape as well as in confinements of arbitrary geometry, especially for application to nanofluidic devices. One of the possible solutions is to build a hybrid scheme with boundary element method[15] into the Stokesian dynamics.[19] Another approach is to replace the free-space Green function (the Oseen-Burgers tensor) by that of the corresponding geometries. For slip surfaces, however, the available solution is limited to a single plane.[30]

Finally, we note that the present formulation is also applicable to microfluidics, too, and many other areas. Actually, the surface slip appears in various situations,[24] including electro-osmosis[2] and non-Newtonian fluids,[58,59] where the results of this article can be used without modifications.

Acknowledgments

This work was supported by the National Research Council (NRC) of Canada. We express our gratitude to Professor D. Jed Harrison for stimulating discussions.

APPENDIX A: LAMB'S GENERAL SOLUTION

Here, we summarize the derivation of the single body problem of the slip spherical particle in terms of Lamb's general solution with the slip boundary condition.

The disturbance field $\boldsymbol{u} - \boldsymbol{u}^\infty$ by the presence of a sphere at the origin is given by Lamb's general solution in Eq. (9). This exerts the disturbance stress field, whose tangential component $(\boldsymbol{I} - \boldsymbol{nn}) \cdot \boldsymbol{\sigma}'$ is given by

$$\begin{aligned}(\boldsymbol{I} - \boldsymbol{nn}) \cdot \boldsymbol{\sigma}' = \frac{\mu}{r} \sum_n \Big\{ & -(n+2)\boldsymbol{\nabla} \times (\boldsymbol{r}\chi_{-n-1}) \\ & -2(n+2)\left(\boldsymbol{\nabla} - \frac{\boldsymbol{r}}{r}\frac{\partial}{\partial r}\right)\Phi_{-n-1} \\ & +\frac{1}{\mu}\frac{(n+1)(n-1)}{n(2n-1)} r^2 \left(\boldsymbol{\nabla} - \frac{\boldsymbol{r}}{r}\frac{\partial}{\partial r}\right) p_{-n-1} \Big\}, \end{aligned} \tag{A1}$$

where χ_n, Φ_n, and p_n are the same functions as in Eq. (9). First, in the slip boundary condition (4), we decompose the disturbance fields and the imposed flows in the following way:

$$\begin{aligned} & \boldsymbol{u}(\boldsymbol{r}) - \boldsymbol{u}^\infty(\boldsymbol{r}) - \frac{\gamma}{\mu}(\boldsymbol{I} - \boldsymbol{nn}) \cdot (\boldsymbol{\sigma}' \cdot \boldsymbol{n}) \\ = \; & (\boldsymbol{U} + \boldsymbol{\Omega} \times \boldsymbol{r}) - (\boldsymbol{U}^\infty + \boldsymbol{\Omega}^\infty \times \boldsymbol{r} + \boldsymbol{E}^\infty \cdot \boldsymbol{r}) \\ & + \frac{\gamma}{\mu}(\boldsymbol{I} - \boldsymbol{nn}) \cdot (\boldsymbol{\sigma}^\infty \cdot \boldsymbol{n}), \end{aligned} \tag{A2}$$

where $\boldsymbol{\sigma}^\infty$ is the stress generated by the imposed flow $\boldsymbol{u}^\infty$. The boundary condition is applied, as in literature,[12,37] through the three scalar functions $(\boldsymbol{r}/r) \cdot \boldsymbol{V}$, $-r\boldsymbol{\nabla} \cdot \boldsymbol{V}$, and $\boldsymbol{r} \cdot \boldsymbol{\nabla} \times \boldsymbol{V}$ for a surface vector $\boldsymbol{V}(\theta, \phi)$ assigned on the surface $r = a$ for a vector field. The disturbance field in the left-hand side in Eq. (A2) is expressed by the coefficients p_{mn}, q_{mn}, and v_{mn} in Eqs. (12), (13), and (14). For the imposed flow in the right-hand side, we introduce the coefficients χ_{mn}, ψ_{mn}, and ω_{mn} as

$$\frac{\boldsymbol{r}}{r} \cdot \boldsymbol{V}^\infty\Big|_{r=a} = \sum_{n=0}^{\infty}\sum_{m=0}^{n} \chi_{mn} Y_{mn}(\theta, \phi), \tag{A3}$$

$$-r\boldsymbol{\nabla} \cdot \boldsymbol{V}^\infty|_{r=a} = \sum_{n=0}^{\infty}\sum_{m=0}^{n} \psi_{mn} Y_{mn}(\theta, \phi), \tag{A4}$$

$$\boldsymbol{r} \cdot \boldsymbol{\nabla} \times \boldsymbol{V}^\infty|_{r=a} = \sum_{n=0}^{\infty}\sum_{m=0}^{n} \omega_{mn} Y_{mn}(\theta, \phi), \tag{A5}$$

where $\boldsymbol{V}^\infty$ denotes the right-hand side in Eq. (A2) on the surface $r = a$. From the boundary condition (A2), then, we have three equations between the coefficients (p_{mn}, q_{mn}, v_{mn}) and $(\chi_{mn}, \psi_{mn}, \omega_{mn})$:

$$\begin{aligned} p_{mn} = \; & \frac{2n-1}{n+1}\Gamma_{0,2n+1}\psi_{mn} \\ & + \frac{(n+2)(2n-1)}{n+1}\Gamma_{2n,2n+1}\chi_{mn}, \end{aligned} \tag{A6}$$

$$\begin{aligned} v_{mn} = \; & \frac{1}{2(n+1)}\Gamma_{0,2n+1}\psi_{mn} \\ & + \frac{n}{2(n+1)}\Gamma_{2(n+1)(n-1)/n,2n+1}\chi_{mn}, \end{aligned} \tag{A7}$$

$$q_{mn} = \frac{1}{n(n+1)}\Gamma_{0,n+2}\omega_{mn}. \tag{A8}$$

From these equations, we can obtain the solution (p_{mn}, q_{mn}, v_{mn}) for each problem specified by the coefficients $(\chi_{mn}, \psi_{mn}, \omega_{mn})$.

APPENDIX B: EWALD SUMMATION

Here, we give full solutions of the mobility matrix in the FTS version under the periodic boundary condition outlined in Sec. II D.

1. Real Space

It is straightforward to obtain the matrix in real-space summation in Eq. (86) from the expressions of each submatrices by the derivatives in Eqs. (54) to (59) and those of $\boldsymbol{R}$ in Eq. (29) and $\boldsymbol{K}$ in Eq. (38) with the Oseen-Burgers tensor in real space $\boldsymbol{J}^{(1)}$ in Eq. (78), whose explicit from is given by

$$J_{ij}^{(1)}(\boldsymbol{r}) = A_0(r,\xi)\delta_{ij} + B_0(r,\xi)\frac{r_i r_j}{r^2}, \tag{B1}$$

where A_0 and B_0 are given by Eqs. (90) and (92), respectively. The scalar functions are given by complementary functions as

$$\begin{aligned}
x_{12}^a &= \mathcal{A}_1^{(0)} + \mathcal{A}_2^{(0)} + \frac{\overline{a_1}^2 + \overline{a_2}^2}{6}\left(\mathcal{A}_1^{(2)} + \mathcal{A}_2^{(2)}\right), && \text{(B2)}\\
y_{12}^a &= \mathcal{A}_1^{(0)} + \frac{\overline{a_1}^2 + \overline{a_2}^2}{6}\mathcal{A}_1^{(2)}, && \text{(B3)}\\
y_{12}^b &= \mathcal{B}_1, && \text{(B4)}\\
x_{12}^c &= C_1 + C_2, && \text{(B5)}\\
y_{12}^c &= C_1, && \text{(B6)}\\
x_{12}^g &= -3\left[\mathcal{G}_1^{(0)} + \left(\frac{\overline{a_1}^2}{10} + \frac{\overline{a_2}^2}{6}\right)\mathcal{G}_1^{(2)}\right], && \text{(B7)}\\
y_{12}^g &= \mathcal{G}_2^{(0)} + \left(\frac{\overline{a_1}^2}{10} + \frac{\overline{a_2}^2}{6}\right)\mathcal{G}_2^{(2)}, && \text{(B8)}\\
y_{12}^h &= \mathcal{H}_1^{(0)}, && \text{(B9)}\\
x_{12}^m &= 6\left[\mathcal{M}_3^{(0)} + \mathcal{M}_5^{(0)} + \frac{\overline{a_1}^2 + \overline{a_2}^2}{10}\left(\mathcal{M}_3^{(2)} + \mathcal{M}_5^{(2)}\right)\right], && \text{(B10)}\\
y_{12}^m &= 2\left[\mathcal{M}_4^{(0)} + \mathcal{M}_5^{(0)} + \frac{\overline{a_1}^2 + \overline{a_2}^2}{10}\left(\mathcal{M}_4^{(2)} + \mathcal{M}_5^{(2)}\right)\right], && \text{(B11)}\\
z_{12}^m &= 2\left(\mathcal{M}_5^{(0)} + \frac{\overline{a_1}^2 + \overline{a_2}^2}{10}\mathcal{M}_5^{(2)}\right). && \text{(B12)}
\end{aligned}$$

The functions for x^a and y^a are

$$\begin{aligned}
\mathcal{A}_1^{(0)} &= \frac{\xi a_\alpha}{\sqrt{\pi}}\left(-\frac{9}{2} + 3r^2\xi^2\right)e^{-\xi^2 r^2} + \frac{3a_\alpha}{4r}\mathrm{erfc}(\xi r), && \text{(B13)}\\
\mathcal{A}_1^{(2)} &= \frac{1}{r^2}\left[\frac{\xi a_\alpha}{\sqrt{\pi}}3\left(1 + 14\xi^2 r^2 - 20\xi^4 r^4 + 4\xi^6 r^6\right)e^{-\xi^2 r^2}\right.\\
&\quad \left. + \frac{3}{2}\frac{a_\alpha}{r}\mathrm{erfc}(\xi r)\right], && \text{(B14)}\\
\mathcal{A}_2^{(0)} &= \frac{\xi a_\alpha}{\sqrt{\pi}}\left(\frac{3}{2} - 3r^2\xi^2\right)e^{-\xi^2 r^2} + \frac{3a_\alpha}{4r}\mathrm{erfc}(\xi r), && \text{(B15)}\\
\mathcal{A}_2^{(2)} &= \frac{1}{r^2}\left[-\frac{\xi a_\alpha}{\sqrt{\pi}}3\left(3 + 2\xi^2 r^2 - 16\xi^4 r^4 + 4\xi^6 r^6\right)e^{-\xi^2 r^2}\right.\\
&\quad \left. - \frac{9}{2}\frac{a_\alpha}{r}\mathrm{erfc}(\xi r)\right]. && \text{(B16)}
\end{aligned}$$

The function for y^b is

$$\mathcal{B}_1 = -\frac{\xi a_\alpha}{\sqrt{\pi}}\frac{3a_\alpha}{2r}\left(1 - 6\xi^2 r^2 + 2\xi^4 r^4\right)e^{-\xi^2 r^2} - \frac{3a_\alpha^2}{4r^2}\mathrm{erfc}(\xi r). \tag{B17}$$

The functions for x^c and y^c are

$$\begin{aligned}
C_1 &= -\frac{\xi a_\alpha}{\sqrt{\pi}}\frac{3a_\alpha^2}{4r^2}\left(1 + 14\xi^2 r^2 - 20\xi^4 r^4 + 4\xi^6 r^6\right)e^{-\xi^2 r^2}\\
&\quad - \frac{3a_\alpha^3}{8r^3}\mathrm{erfc}(\xi r) && \text{(B18)}\\
C_2 &= \frac{\xi a_\alpha}{\sqrt{\pi}}\frac{3a_\alpha^2}{4r^2}\left(3 + 2\xi^2 r^2 - 16\xi^4 r^4 + 4\xi^6 r^6\right)e^{-\xi^2 r^2}\\
&\quad + \frac{9a_\alpha^3}{8r^3}\mathrm{erfc}(\xi r) && \text{(B19)}
\end{aligned}$$

The functions for x^g and y^g are

$$\begin{aligned}
\mathcal{G}_1^{(0)} &= \frac{\xi a_\alpha}{\sqrt{\pi}}\frac{3a_\alpha}{2r}\left(-1 + 2\xi^2 r^2\right)e^{-\xi^2 r^2} - \frac{3a_\alpha^2}{4r^2}\mathrm{erfc}(\xi r) && \text{(B20)}\\
\mathcal{G}_1^{(2)} &= \frac{1}{r^2}\left[\frac{\xi a_\alpha}{\sqrt{\pi}}\frac{3a_\alpha}{r}\left(3 + 2\xi^2 r^2 - 16\xi^4 r^4 + 4\xi^6 r^6\right)e^{-\xi^2 r^2}\right.\\
&\quad \left. + \frac{9a_\alpha^2}{2r^2}\mathrm{erfc}(\xi r)\right], && \text{(B21)}\\
\mathcal{G}_2^{(0)} &= \frac{\xi a_\alpha}{\sqrt{\pi}}3\xi^2 a_\alpha r\left(-2 + \xi^2 r^2\right)e^{-\xi^2 r^2} && \text{(B22)}\\
\mathcal{G}_2^{(2)} &= \frac{1}{r^2}\left[\frac{\xi a_\alpha}{\sqrt{\pi}}\frac{3a_\alpha}{r}\left(3 + 2\xi^2 r^2 + 26\xi^4 r^4 - 26\xi^6 r^6 + 4\xi^8 r^8\right)e^{-\xi^2 r^2}\right.\\
&\quad \left. + \frac{9a_\alpha^2}{2r^2}\mathrm{erfc}(\xi r)\right], && \text{(B23)}
\end{aligned}$$

The function for y^h is

$$\begin{aligned}
\mathcal{H}_1^{(0)} &= -\frac{\xi a_\alpha}{\sqrt{\pi}}\frac{3a_\alpha^2}{4r^2}\left(3 + 2\xi^2 r^2 - 16\xi^4 r^4 + 4\xi^6 r^6\right)e^{-\xi^2 r^2}\\
&\quad - \frac{9a_\alpha^3}{8r^3}\mathrm{erfc}(\xi r). && \text{(B24)}
\end{aligned}$$

The functions for x^m, y^m, and z^m are

$$\begin{aligned}
\mathcal{M}_3^{(0)} &= -\frac{\xi a_\alpha}{\sqrt{\pi}}\frac{3a_\alpha^2}{2r^2}\left(1 - 2\xi^2 r^2\right)e^{-\xi^2 r^2} - \frac{3a_\alpha^3}{4r^3}\mathrm{erfc}(\xi r) && \text{(B25)}\\
\mathcal{M}_3^{(2)} &= \frac{1}{r^2}\left[\frac{\xi a_\alpha}{\sqrt{\pi}}\frac{3a_\alpha^2}{10r^2}\left(3 + 2\xi^2 r^2 - 16\xi^4 r^4 + 4\xi^6 r^6\right)e^{-\xi^2 r^2}\right.\\
&\quad \left. + \frac{9a_\alpha^3}{20r^3}\mathrm{erfc}(\xi r)\right], && \text{(B26)}
\end{aligned}$$

$$\mathcal{M}_4^{(0)} = \frac{\xi a_\alpha}{\sqrt{\pi}} \frac{3a_\alpha^2}{4r^2} \left(3 + 2\xi^2 r^2 + 8\xi^4 r^4 - 4\xi^6 r^6\right) e^{-\xi^2 r^2} + \frac{9a_\alpha^3}{8r^3} \mathrm{erfc}(\xi r) \tag{B27}$$

$$\mathcal{M}_4^{(2)} = \frac{1}{r^2} \left[-\frac{\xi a_\alpha}{\sqrt{\pi}} \frac{3a_\alpha^2}{10r^2} \left(15 + 10\xi^2 r^2 + 4\xi^4 r^4 + 32\xi^6 r^6 - 30\xi^8 r^8 + 4\xi^{10} r^{10}\right) e^{-\xi^2 r^2} - \frac{9a_\alpha^3}{4r^3} \mathrm{erfc}(\xi r) \right], \tag{B28}$$

$$\mathcal{M}_5^{(0)} = \frac{\xi a_\alpha}{\sqrt{\pi}} 3\xi^2 a_\alpha^2 \left(-2 + \xi^2 r^2\right) e^{-\xi^2 r^2} \tag{B29}$$

$$\mathcal{M}_5^{(2)} = \frac{1}{r^2} \left[\frac{\xi a_\alpha}{\sqrt{\pi}} \frac{3a_\alpha^2}{10r^2} \left(3 + 2\xi^2 r^2 + 26\xi^4 r^4 - 26\xi^6 r^6 + 4\xi^8 r^8\right) e^{-\xi^2 r^2} + \frac{9a_\alpha^3}{20r^3} \mathrm{erfc}(\xi r) \right]. \tag{B30}$$

2. Reciprocal Space

Fourier transform of the Oseen-Burgers tensor in the reciprocal part $\boldsymbol{J}^{(2)}$ is

$$\widetilde{J}_{ij}(k) = \int \mathrm{d}\boldsymbol{r}\; e^{\mathrm{i}\boldsymbol{k}\cdot\boldsymbol{r}} J_{ij}^{(2)}(\boldsymbol{r}) = \left(\delta_{ij} - \hat{k}_i \hat{k}_j\right) k^2 \mathcal{J}(k), \tag{B31}$$

where $\hat{\boldsymbol{k}} = \boldsymbol{k}/|\boldsymbol{k}|$ and

$$\mathcal{J}(k) = \frac{8\pi}{k^4} \left(1 + \frac{k^2}{4\xi^2} + \frac{k^4}{8\xi^4}\right) \exp\left(-\frac{k^2}{4\xi}\right). \tag{B32}$$

With this expression and Eqs. (54) to (59), the submatrices are obtained as

$$a_{ij}^{(2)} = \frac{3a_\alpha}{4} \left(1 - k^2 \frac{\overline{a_\alpha}^2 + \overline{a_\beta}^2}{6}\right) \left(\delta_{ij} - \hat{k}_i \hat{k}_j\right) k^2 \mathcal{J}(k), \tag{B33}$$

$$b_{ij}^{(2)} = \frac{3a_\alpha^2}{8} (-i) \epsilon_{ijk} \hat{k}_k k^3 \mathcal{J}(k), \tag{B34}$$

$$c_{ij}^{(2)} = \frac{3a_\alpha^3}{16} \left(\delta_{ij} - \hat{k}_i \hat{k}_j\right) k^4 \mathcal{J}(k), \tag{B35}$$

$$g_{ijk}^{(2)} = -\frac{3a_\alpha^2}{8} \left[1 - k^2 \left(\frac{\overline{a_\alpha}^2}{10} + \frac{\overline{a_\beta}^2}{6}\right)\right] (-i) \left(\hat{k}_j \delta_{ik} + \delta_{jk} \hat{k}_i - 2\hat{k}_i \hat{k}_j \hat{k}_k\right) k^3 \mathcal{J}(k), \tag{B36}$$

$$h_{ijk}^{(2)} = \frac{3a_\alpha^3}{16} \left(\epsilon_{ikl} \hat{k}_j \hat{k}_l + \epsilon_{jkl} \hat{k}_i \hat{k}_l\right) k^4 \mathcal{J}(k), \tag{B37}$$

$$m_{ijkl}^{(2)} = \frac{3a_\alpha^3}{16} \left(1 - k^2 \frac{\overline{a_\alpha}^2 + \overline{a_\beta}^2}{10}\right) \left(\hat{k}_j \hat{k}_l \delta_{ik} + \hat{k}_j \hat{k}_k \delta_{il} + \hat{k}_i \hat{k}_l \delta_{jk} + \hat{k}_i \hat{k}_k \delta_{jl} - 4\hat{k}_i \hat{k}_j \hat{k}_k \hat{k}_l\right) k^4 \mathcal{J}(k). \tag{B38}$$

Thus, Eq. (94) has been derived.

3. Self Term in Reciprocal Space

The self term in reciprocal part is evaluated by the inverse Fourier transform of the reciprocal part obtained in the previous section.

Because the submatrices $\boldsymbol{b}^{(2)}$ and $\boldsymbol{g}^{(2)}$ are odd functions of $\boldsymbol{k}$ as shown in Eqs. (B34) and (B36), they go to zero. Although $\boldsymbol{h}^{(2)}$ is an even function of $\boldsymbol{k}$ as in Eq. (B37), the angle integral gives

$$\int \mathrm{d}\hat{\boldsymbol{k}} \left(\epsilon_{ilj} \hat{k}_l \hat{k}_k + \epsilon_{ilk} \hat{k}_l \hat{k}_j\right) = \frac{4\pi}{3} \left(\epsilon_{ilj} \delta_{lk} + \epsilon_{ilk} \delta_{lj}\right) = 0, \tag{B39}$$

so that it also vanishes. Therefore, only $\boldsymbol{a}^{(2)}$, $\boldsymbol{c}^{(2)}$, $\boldsymbol{m}^{(2)}$ are left.

To evaluate $\boldsymbol{a}^{(2)}$, let us split the integral into two parts, radial integral for k and solid-angle integral for $\hat{\boldsymbol{k}}$. From Eq. (B33),

$$a_{ij}^{(2)}(\boldsymbol{r} = \boldsymbol{0}) = \frac{1}{(2\pi)^3} \int_0^\infty \mathrm{d}k\; \frac{3a_\alpha}{4} \left(1 - \frac{\overline{a_\alpha}^2 + \overline{a_\beta}^2}{6} k^2\right) k^4 \mathcal{J}(k) \times \int \mathrm{d}\hat{\boldsymbol{k}} \left(\delta_{ij} - \hat{k}_i \hat{k}_j\right). \tag{B40}$$

To calculate the radial integrals, we use the recurrence relation $G_n = 2(2n-1)\xi^2 G_{n-1}$ with the initial condition $G_0 = \xi\sqrt{\pi}$ for G_n defined by

$$G_n = \int_0^\infty \mathrm{d}k\; k^{2n} e^{-k^2/4\xi^2}. \tag{B41}$$

The radial integral for $\boldsymbol{a}^{(2)}$ is, then,

$$\frac{1}{(2\pi)^3} \int_0^\infty \mathrm{d}k\; \frac{3a_\alpha}{4} \left(1 - \frac{\overline{a_\alpha}^2 + \overline{a_\beta}^2}{6} k^2\right) k^4 \mathcal{J}(k) = \frac{1}{\pi^{3/2}} \frac{3a_\alpha \xi}{4} \left(3 - 20\xi^2 \frac{\overline{a_\alpha}^2 + \overline{a_\beta}^2}{6}\right). \tag{B42}$$

The angle integral is

$$\int \mathrm{d}\hat{\boldsymbol{k}} \left(\delta_{ij} - \hat{k}_i \hat{k}_j\right) = 4\pi \left(1 - \frac{1}{3}\right) \delta_{ij}. \tag{B43}$$

Therefore, Eq. (95) is obtained:

$$a_{ij}^{(2)}(\boldsymbol{r} = \boldsymbol{0}) = \frac{a_\alpha \xi}{\sqrt{\pi}} \left(6 - 20\xi^2 \frac{\overline{a_\alpha}^2 + \overline{a_\beta}^2}{3}\right) \delta_{ij}. \tag{B44}$$

For $\boldsymbol{c}^{(2)}$, from Eq. (B35) we have

$$c_{ij}^{(2)}(\boldsymbol{r} = \boldsymbol{0}) = \frac{3a_\alpha^3}{16} \frac{1}{(2\pi)^3} \int_0^\infty \mathrm{d}k\; k^6 \mathcal{J}(k) \times \int \mathrm{d}\hat{\boldsymbol{k}} \left(\delta_{ij} - \hat{k}_i \hat{k}_j\right). \tag{B45}$$

The radial integral is

$$\frac{3a_\alpha^3}{16} \frac{1}{(2\pi)^3} \int_0^\infty \mathrm{d}k\; k^6 \mathcal{J}(k) = \frac{15a_\alpha^3}{4} \frac{\xi^3}{\pi^{3/2}}. \tag{B46}$$

The angle integral is the same for $a_{ij}^{(2)}$. Therefore,

$$c_{ij}^{(2)}(\boldsymbol{r}=\boldsymbol{0}) = \frac{10a_\alpha^3\xi^3}{\sqrt{\pi}}\delta_{ij}. \tag{B47}$$

For $\boldsymbol{m}^{(2)}$, from Eq. (B38),

$$\begin{aligned} m_{ij}^{(2)}(\boldsymbol{r}=\boldsymbol{0}) &= \frac{3a_\alpha^3}{16}\frac{1}{(2\pi)^3}\int_0^\infty \mathrm{d}k\left[1-\frac{k^2}{10}\left(\overline{a_\alpha}^2+\overline{a_\beta}^2\right)\right]k^6\mathcal{J}(k) \\ &\times\int \mathrm{d}\hat{\boldsymbol{k}}\left(\hat{k}_j\hat{k}_l\delta_{ik}+\hat{k}_j\hat{k}_k\delta_{il}\right. \\ &\left.+\hat{k}_i\hat{k}_l\delta_{jk}+\hat{k}_i\hat{k}_k\delta_{jl}-4\hat{k}_i\hat{k}_j\hat{k}_k\hat{k}_l\right). \end{aligned} \tag{B48}$$

The radial integral is

$$\begin{aligned} &\frac{3a_\alpha^3}{16}\frac{1}{(2\pi)^3}\int_0^\infty \mathrm{d}k\left[1-\frac{k^2}{10}\left(\overline{a_\alpha}^2+\overline{a_\beta}^2\right)\right]k^6\mathcal{J}(k) \\ &= \frac{3a_\alpha^3}{16}\frac{1}{\pi^{3/2}}\left[20\xi^3-\frac{126}{5}\xi^5\left(\overline{a_\alpha}^2+\overline{a_\beta}^2\right)\right]. \end{aligned} \tag{B49}$$

The angle integral gives

$$\begin{aligned} &\int \mathrm{d}\hat{\boldsymbol{k}}\left(\hat{k}_j\hat{k}_l\delta_{ik}+\hat{k}_j\hat{k}_k\delta_{il}+\hat{k}_i\hat{k}_l\delta_{jk}+\hat{k}_i\hat{k}_k\delta_{jl}-4\hat{k}_i\hat{k}_j\hat{k}_k\hat{k}_l\right) \\ &= \frac{8\pi}{5}\left\{\left(\delta_{jl}\delta_{ik}+\delta_{jk}\delta_{il}\right)-\frac{2}{3}\delta_{ij}\delta_{kl}\right\}, \end{aligned} \tag{B50}$$

where we use the result[21]

$$\int \mathrm{d}\hat{\boldsymbol{k}}\,\hat{k}_i\hat{k}_j\hat{k}_k\hat{k}_l = \frac{4\pi}{15}\left(\delta_{ij}\delta_{kl}+\delta_{ik}\delta_{jl}+\delta_{il}\delta_{jk}\right). \tag{B51}$$

Therefore,

$$\begin{aligned} m_{ij}^{(2)}(\boldsymbol{r}=\boldsymbol{0}) &= \frac{a_\alpha^3\xi^3}{\sqrt{\pi}}\left[6-\frac{189}{25}\xi^2\left(\overline{a_\alpha}^2+\overline{a_\beta}^2\right)\right] \\ &\times\left\{\left(\delta_{jl}\delta_{ik}+\delta_{jk}\delta_{il}\right)-\frac{2}{3}\delta_{ij}\delta_{kl}\right\}. \end{aligned} \tag{B52}$$

The corresponding scalar functions are

$$x_{\alpha\beta}^{m(2)} = y_{\alpha\beta}^{m(2)} = z_{\alpha\beta}^{m(2)} = \frac{a_\alpha^3\xi^3}{\sqrt{\pi}}\left[12-\frac{378}{25}\xi^2\left(\overline{a_\alpha}^2+\overline{a_\beta}^2\right)\right]. \tag{B53}$$

1. T. M. Squires and S. R. Quake, *Rev. Mod. Phys.* 77, 977 (**2005**).
2. H. A. Stone, A. D. Stroock, and A. Ajdari, *Annu. Rev. Fluid Mech.* 36, 381 (**2004**).
3. J. C. T. Eijkel and A. van den Berg, *Microfluid Nanofluid* 1, 249 (**2005**).
4. G. Karniadakis, A. Beskok, and N. Aluru, *Mircoflows and Nanoflows*, Springer, New York, (**2005**).
5. L. R. Huang, E. C. Cox, R. H. Austin, and J. C. Sturm, *Science* 304, 987 (**2004**).
6. J. A. Davis, D. W. Inglis, K. J. Morton, D. A. Lawrence, L. R. Huang, S. Y. Chou, J. C. Sturm, and R. H. Austin, *Proc. Natl. Acad. Sci. U.S.A.* 103, 14779 (**2006**).
7. D. Hun, J. H. Bahng, Y. Ling, H.-H. Wei, O. D. Kripfgans, J. B. Fowlkes, J. B. Grotberg, and S. Takayama, *Anal. Chem.* 79, 1369 (**2007**).
8. H. Bayley and P. S. Cremer, *Nature* 413, 226 (**2001**).
9. C. R. Martin, M. Nishizawa, K. Jirage, and M. Kang, *J. Phys. Chem. B* 105, 1925 (**2001**).
10. G. Woodhouse, L. King, L. Wieczorek, P. Osman, and B. Cornell, *J. Mol. Recognit.* 12, 328 (**1999**).
11. K. P. Travis, B. D. Todd, and D. J. Evans, *Phys. Rev. E* 55, 4288 (**1997**).
12. J. Happel and H. Brenner, *Low Reynolds Number Hydrodynamics*, Martunus Nihhoff, Dordrecht, (**1973**).
13. S. Kim and S. J. Karrila, *Microhydrodynamics*, Butterworth-Heinemann, Boston, (**1991**).
14. W. B. Russel, D. A. Saville, and W. R. Schowalter, *Colloidal Dispersions*, Cambridge University Press, Cambridge, (**1989**).
15. C. Pozrikidis, *Boundary Integral and Singularity Methods for Linearized Viscous Flow*, Cambridge University Press, Cambridge, (**1992**).
16. J. F. Brady and G. Bossis, *Annu. Rev. Fluid Mech.* 20, 111 (**1988**).
17. L. Durlofsky, J. F. Brady, and G. Bossis, *J. Fluid Mech.* 180, 21 (**1987**).
18. J. F. Brady, R. J. Phillips, J. C. Lester, and G. Bossis, *J. Fluid Mech.* 195, 257 (**1988**).
19. L. J. Durlofsky and J. F. Brady, *J. Fluid Mech.* 200, 39 (**1989**).
20. A. Sierou and J. F. Brady, *J. Fluid Mech.* 448, 115 (**2001**).
21. K. Ichiki, *J. Fluid Mech.* 452, 231 (**2002**).
22. A. J. Banchio and J. F. Brady, *J. Chem. Phys.* 118, 10323 (**2003**).
23. R. D. Groot and P. B. Warren, *J. Chem. Phys.* 107, 4423 (**1997**).
24. E. Lauga, M. P. Brenner, and H. A. Stone, in *Springer Handbook of Experimental Fluid Dynamics*, Edited C. Tropea, A.L. Yarin, and J.F. Foss, Springer, Berlin, (**2007**), Chapter 19, pp. 1219–1240.
25. C. Neto, D. R. Evans, E. Bonaccurso, H.-J. Butt, and V. S. G. Craig, *Rep. Prog. Phys.* 68, 2859 (**2005**).
26. O. I. Vinogradova, *Int. J. Miner. Process.* 56, 31 (**1999**).
27. E. Lauga and H. A. Stone, *J. Fluid Mech.* 489, 55 (**2003**).
28. M. Navier, *Mem. Acad. R. Sci. Inst. France* 6, 389 (**1823**).
29. J. C. Maxwell, *Phil. Trans. Roy. Soc. Lond.* 170, 231 (**1879**).
30. E. Lauga and T. M. Squires, *Phys. Fluids* 17, 103102 (**2005**).
31. K. Ichiki and H. Hayakawa, *Phys. Rev. E* 52, 658 (**1995**).
32. A. B. Basset, *A Treatise on Hydrodynamics, Vol 2*, Dover, New York, (**1961**).
33. B. U. Felderhof, *Physica A* 84, 569 (**1976**).
34. B. U. Felderhof, *Physica A* 89, 373 (**1977**).

35. J. Bławzdziewicz, E. Wajnryb, and M. Loewenberg, *J. Fluid Mech.* 395, 29 (**1999**).
36. H. Luo and C. Pozrikidis, *J. Fluid Mech.* 581, 129 (**2007**).
37. D. J. Jeffrey and Y. Onishi, *J. Fluid Mech.* 139, 261 (**1984**).
38. R. Ying and M. H. Peters, *J. Fluid Mech.* 207, 353 (**1989**).
39. H. J. Keh and S. H. Chen, *Chem. Eng. Sci.* 52, 1789 (**1997**).
40. K. Ichiki (**2007**), in preparation.
41. J. R. Blake, *Proc. Camb. Phil. Soc.* 70, 303 (**1971**).
42. H. Lamb, *Hydrodynamics*, Cambridge University Press, Cambridge, (**1932**).
43. B. S. Padmavathi, T. Amaranath, and S. D. Nigam, *Fluid Dyn. Res.* 11, 229 (**1993**).
44. D. J. Jeffrey, *Phys. Fluids A* 4, 16 (**1992**).
45. C. W. J. Beenakker, *J. Chem. Phys.* 85, 1581 (**1986**).
46. K. R. Hase and R. L. Powell, *Phys. Fluids* 13, 32 (**2001**).
47. H. Hasimoto, *J. Fluid Mech.* 5, 317 (**1959**).
48. G. K. Batchelor, *J. Fluid Mech.* 52, 245 (**1972**).
49. A. A. Zick and G. M. Homsy, *J. Fluid Mech.* 115, 13 (**1982**).
50. M. Zuzovsky, P. M. Adler, and H. Brenner, *Phys. Fluids* 26, 1714 (**1983**).
51. K. C. Nunan and J. B. Keller, *J. Fluid Mech.* 142, 269 (**1984**).
52. D. Nykypanchuk, H. H. Strey, and D. A. Hoagland, *Science* 297, 987 (**2002**).
53. Z. Li and G. Drazer, *Phys. Rev. Lett.* 98, 050602 (**2007**).
54. D. L. Ermak and J. A. McCammon, *J. Chem. Phys.* 69, 1352 (**1978**).
55. M. Fixman, *J. Chem. Phys.* 69, 1527 (**1978**).
56. G. Bossis and J. F. Brady, *J. Chem. Phys.* 87, 5437 (**1987**).
57. T. N. Phung, J. F. Brady, and G. Bossis, *J. Fluid Mech.* 313, 181 (**1996**).
58. P. G. De Gennes, *C. R. Acad. Sci. Paris B* 288, 291 (**1979**).
59. F. Brochard and P. G. De Gennes, *Langmuir* 8, 3033 (**1992**).